Unsteady Aerodynamic Vortex Lattice of Moving Aircraft

September 30, 2011

Master thesis

Author:
Enrique Mata Bueso

Supervisors:
Arthur Rizzi
Jesper Oppelstrup

Aeronautical and Vehicle engineering department, KTH, Kungliga Tekniska Högskolan

SE-100 44 Stockholm, Sweden

Contents

Nomenclature

D	Aerodynamic drag.
L	Lift force.
T	Thrust.
W	Weight of the flying body.
Δp_{ij}	Pressure on a panel of the lifting surface.
$\bar{c}$	Mean aerodynamic chord of the aircraft.
$\boldsymbol{V}_\infty$	Free stream velocity.
$\boldsymbol{\Gamma}$	Circulation.
$\boldsymbol{l}$	Lift per unit width.
$\mathbf{C}$	Velocity of the aircraft in the inertial system of reference
$\mathbf{V}$	Velocity vector of the free-stream in the inertial system of reference
$\boldsymbol{\Omega}$	Angular frequency.
$\boldsymbol{\Theta}$	Rate angles vector
ρ	Air density.
b_{ref}	Span of the main wing of the aircraft. Also called reference span.
g	Gravity constant ($9.81 m/s^2$).
k	Reduced frequency $k = \frac{\Omega c}{2V_\infty}$
p	Pressure.
u	Velocity of the aircraft in X-direction in the inertial frame of reference
v	Velocity of the aircraft in Y-direction in the inertial frame of reference
w	Velocity of the aircraft in Z-direction in the inertial frame of reference
z	Altitude.
$\bar{c}$	Mean aerodynamic chord of the aircraft.

List of Figures

List of Tables

Abstract

It is aim of this thesis to develop a potential flow solver for unsteady aerodynamics in MATLAB environment. In order to achieve this target a vortex lattice method based has been developed. The validation of this program involves two different stages. Initially, it is compared with classical experiments and a well tested code. In a second step, the program is compared with wind tunnel experiments for two different aircraft's configurations, classical and with canard. In the end it will be demonstrated that the present method achieves good agreement in both stages.

-

Chapter 1

Introduction

"In the beginning there was nothing, and it exploded."

Terry Pratchett, writer, on the Big Bang theory.

Since the beginning of computational aerodynamics research there have been two different lines of development; one towards accuracy and other towards time efficiency. Navier-Stokes and Euler equations solvers can be included In the first trend. Although they are highly accurate, they involve computational times that are inefficient for early stages of aircraft design. That leads to the second trend, in which potential flow solvers are widely used. Within them, the well-known Vortex Lattice method can be found. Its main strengths lie on low computational times and robust solutions that achieve reasonably good approximations under linear aerodynamics conditions.

The last case is the target of this Master thesis. An unsteady vortex lattice method is developed due to a requirement of the Aerodynamics division at the Royal Institute of Technology of Sweden (KTH). It is referred as ABSOLUT (Aerodynamic Boundaryless SOLver for Unsteady Terms) because is able to calculate the aerodynamic coefficients, forces and moments under unsteady conditions. Its steady part is based on Tornado [32], built initially by Tomas Melin, also in KTH. For the unsteady solver, the present code finds its source in Hedring [10], a basic program developed by Sven Hedman, specifically created to solve the cases in chapter 4.

1.1 CEASIOM

CEASIOM (Computerised Environment for Aircraft Synthesis and Integrated Optimization Methods) is a computational aircraft pre-design tool. It appears as new way of understanding the computer aid to conceptual design of aircrafts [30]. Most of current commercial software in this field tends to use semi-empirical theory which can be found in well-known handbooks. Some of them, sophisticated ones, even recalibrate these methods and data by using experimental tests, previous designs and projects. However, the final product is not as reliable as it is desired for unconventional configurations. Due to the need of filling this gap, it arises the SimSAC project [31], frame of CEASIOM development. Its main objective is to build new software that performs initial fast non-high accuracy analysis but capable of introducing higher accurate numerical simulations, when requested.

Since it is an international project, CEASIOM system is not unique software, but it is an integration of different analysis modules by using common tool MATLAB software. Therefore, although it is freeware software, a MATLAB license is necessary to use it.

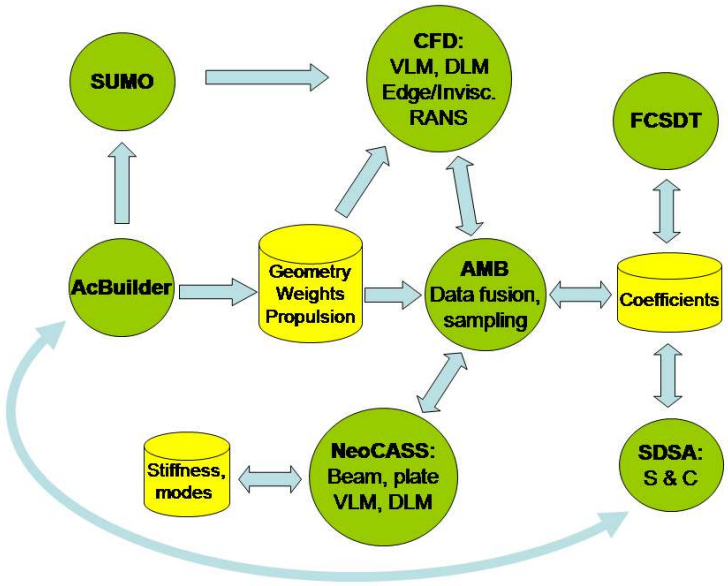

Figure 1.1: Overview of the different modules of CEASIOM

The different modules and their interactions are shown in fig.1.1, obtained from [30]. Each one is related to a specific aspect of conceptual design. These modules are:

- **AcBuilder/SUMO**: it is the CAD package. It is a coupled system of geometry construction and mesh generators. Its main characteristic is the adaptable quality of the different geometries and meshes. Depending on the aerodynamic method that is going to be executed, different files can be created. A geo.xml file defined with the AcBuilder GUI is sufficient for a first approxiamtion. Lifting surfaces are modeled as lamina assembled through their usual aerodynamic defining geometries. Control surface deflections can be modeled by changing the geometry or by manipulating the numerical flow conditions. The non-lifting elements have only a few key parameters, and their effects on the lifting surfaces are approximated by the slender body theory. For higher geometry fidelity, SUMO package provides the proper refinement routines from which surface and volume mesh files .msh come.

- **AMB**: as its abbreviation indicates, it is the Aircraft Model Builder. It deals with the aerodynamic calculations for a given geometry from the CAD module. The computational models are dvided into three groups:

  (a) **(Tier I)**: Linear Aerodynamics methods, (mainly Vortex Lattice Method) that in this case cover low speeds and low angles of attack of the aircraft. The main tool in this model is TORNADO, which is a VLM code that allows most types of modern aircraft configurations, from the airfoil characteristics to the control surfaces. It also calculates forces, moments and the aerodynamic coefficients. The aerodynamic derivatives can be calculated with respect to: angle of attack, angle of sideslip, roll, pitch, yaw rotations, and control surface deflections. Although both viscous and aeroelastic effects are supposed to be obtained, only viscous corrections are implemented by using the airfoil code XFOIL [33]. The aeroelasticity version is still under development. Also USAF digital DATCOM handbook methods can be used as basic tool.

  (b) **(Tier I+)**: For high-speed aerodynamics and aeroelasticity. For this case there are two different possibilities. The first is to solve the problem with Panel method by using dwfsolve from SUMO surface mesh file which has been also created from a AcBuilder output. The second is to use EDGE code from TetGen's volume mesh files to obtain the transonic aerodata. Both methods are highly accurate.

(c) **(Tier II)**: RANS (Reynolds-averaged Navier-Stokes method). This high-fidelity analysis allows to extract accurate solutions from extreme flight conditions. However, it requires much more work than the two previous, not only in the creation of the mesh but also in computing time cost.

- **SDSA**(Simulation and Dynamic Stability Analysis): this module can execute many different analyses. The main ones are:

  (a) Stability analysis: It covers eigenvalues analysis in open and close loop case and time history identification. The model is linearized by using the Jacobian matrix of the state derivatives around the equilibrium point numerically.

  (b) Six Degree of Freedom: test flights and turbulence.

  (c) Flight Control System based on Linear Quadratic Regulator (LQR) theory, which includes Human Pilot model, Stability Augmentation System, and Actuator model or LQR based FCS.

  (d) Performance prediction.

- **FCDST**(The Flight Control System design module): it is a module for simulating the aircraft control system so it can be integrated in the architecture from the beginning of the design.

- **NeoCASS**: this module allows structural analysis of the aeroelastic behavior of the aircraft in an early phase of the design. It is based on numerical analysis, which is an improvement in relation to old semi-empirical methods.

1.2 TORNADO, a brief overview

TORNADO is a potential flow solver developed as a collaboration between the Royal Institute of Technology (KTH), University of Bristol and Linköping University. Since the beginning its main purpose is to be used as a tool in conceptual aircraft design and in aerodynamics education [32]. Although the code has been initially developed by Tomas Melin [21] many extensions have been added to improve the basic version.

Tornado uses a vortex lattice method that calculates forces, moments and aerodynamic coefficients of the aircraft for low speeds and low angles of attack. It can also study several modern aircraft configurations, from the airfoil characteristics to the control surfaces. For viscous effects, it works together with Xfoil [33] or with semi-empirical methods. The main features that differentiate it from classical vortex lattice codes are related to the geometry definition and an extension for the theoretical solution.

The geometry definition is three-dimensional with multiple wings configurations allowed. There is the possibility of specifying the characteristics of each section of the wing. These are twist, sweep, dihedral angles, and the existence of control surfaces. Also, different mean camber lines can be used according to the profiles selected for a certain section. Therefore, an aircraft can be defined with multiple wings, with multiple control surfaces in each wing, and different parameters for each section. All of it in three dimensional fashion.

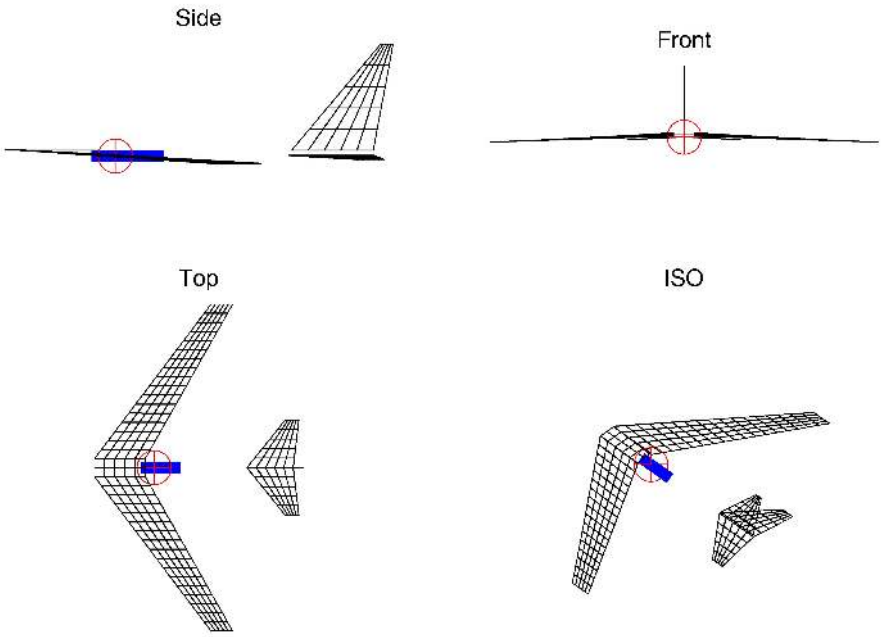

Figure 1.2: Tornado's different views of the B-52

For the theoretical solution, the vortex-sling concept has been developed as an extension of the classical horseshoe. Instead of three straight vortex segments, the new model consists of seven vortex lines for each panel. The vortex sling starts downstream, in the infinity, reaching the trailing edge of the wing, going across it until the quarter chord line of its panel. Then, it goes to the other side of the panel and afterwards back downstream in an analogous way [32]. In case there is a control surface in the section in which the panel is located, the vortex lines moves first to the hinge line of the control surface before it goes to the quarter chord line. This improvement allows to add the effect of control surfaces to the vortex lattice method, which is not possible in classical configurations. In Fig. 1.3 both a horseshoe vortex and a vortex sling are shown side by side so the differences become clearer.

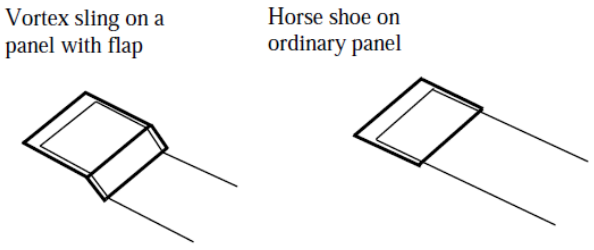

Figure 1.3: Vortex sling vs horseshoe vortex, [21]

The increase in computational time is balance by the increase in accuracy and the possibility of adding control surfaces. Tornado has other minor features and extensions that the following list briefly covers:

- Explicit forces in Newton's.
- Treffz's plane analysis.
- International standard atmosphere.
- Velocity in TAS, CAS or Mach.
- Compressibility corrections for high subsonic Mach numbers.
- Trimmed polars
- Stability derivatives with respect to:
  - Pitch and yaw
  - Angular rates in pitch, roll and yaw.
- Control surface power derivatives
- Parameter sweep

For an updated list, see [32].

1.3 Linear Aerodynamics

Linear aerodynamics theory covers the cases in which the non-linear effects can be neglected. Hence, its domain includes small angles of attack (not close to stall limit, Fig. 1.4), and Mach numbers low enough so compressibility effects are not accounted. In Fig. 1.5 it can be appreciated that from Mach=0.5 the zero-lift drag suffers a progressively sharper increase. Consequently, small disturbances-theory can be used under the assumption of small deviations from an equilibrium state of the aircraft.

The Vortex lattice method is included in the linear aerodynamic methods due to its dependence on the Laplace's equation. This has to be satisfied to solve the aerodynamic problem. This relations are explained in chapter 2.

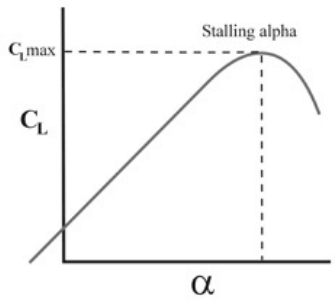

Figure 1.4: Stall limit in a lift-angle of attack curve

In the following sections, diverse examples of linear aerodynamics are depicted in relation to the unsteadiness of the fluid surrounding the body. A first approach shows that if the motion of a wing, in a free stream, changes by time, so do the acting aerodynamic coefficients [9]. If this change is fast enough, the aerodynamic response of the body has a phase lag, and the inertia of the displaced air contributes as an apparent mass term. In case the mass term is negligible, the aerodynamic analysis can be performed under the quasi-unsteady assumption.

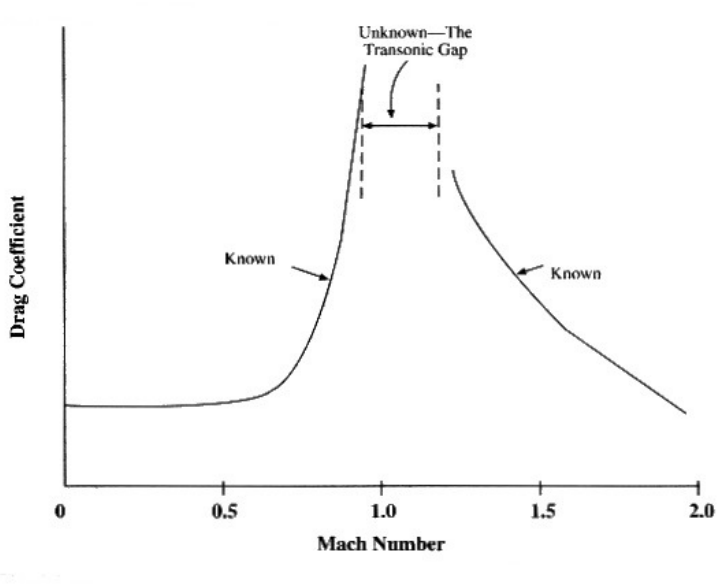

Figure 1.5: Compressibility effects on the drag according to Potential Flow theory

1.3.1 Steady Aerodynamics

For steady aerodynamics, the flow field around a flying body does not change with respect to time. Therefore, the aerodynamic forces and moments keep unchanged along the body's trajectory. An example of this case is an aircraft following a steady, straight and level, unaccelerated flight. From a dynamic point of view, the main forces acting on the aircraft are lift **L**, weight **W**, drag **D** and thrust **T**. The lift balances the weight of the aircraft and the thrust balances the drag.

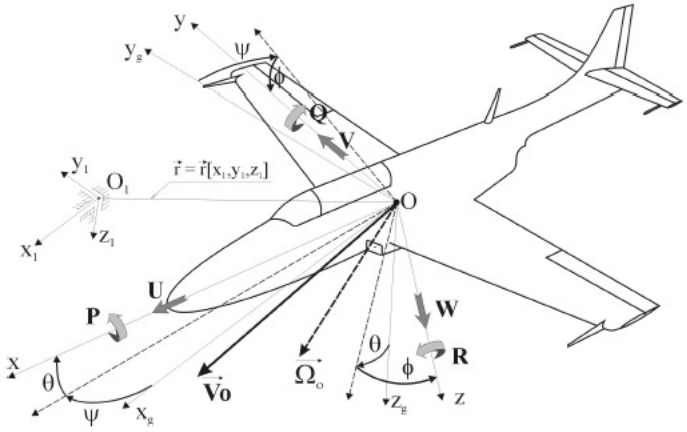

Figure 1.6: Reference system according to CEASIOM definitions [8]

Usually, there is an angle ϵ between the thrust $\boldsymbol{T}$ an the velocity $\mathbf{V}_0$ directions, but this is often neglected ($\epsilon \approx 0$) because it is small enough, Eq. (1.1). For this case, the aerodynamic study only concerns the static situation of the airplane, what means that only its steady parameters are accounted for the calculation. The wake remains unchanged.

$$\begin{aligned} L - W + T\cancel{sin(\epsilon)}^{0} = 0 \rightarrow L - W = 0 \\ T\cancel{cos(\epsilon)}^{1} - D = 0 \rightarrow T - D = 0 \end{aligned} \tag{1.1}$$

In the kinematic analysis, there are only constant straight velocities $\mathbf{V}$ so angular rates $\boldsymbol{\Omega}$ are set to zero, Eq. (1.2).

$$\begin{aligned} \mathbf{V} &= (u_0, v_0, w_0) \\ \mathbf{\Omega} &= (P, Q, R) = (0, 0, 0) \end{aligned} \tag{1.2}$$

where P, Q and R are the roll, pitch and yaw angular velocities, defined as in Fig. 1.6.

1.3.2 Quasi-steady Aerodynamics

When the aircraft undergoes a general motion of pitch, roll and/or yaw, the forces and moments vary with time. One simple approach for the calculation of such forces and moments is to assume that at any instant the wing behaves as if it were moving with constant angular rates equal to their instantaneous values. This is known as the quasi-steady assumption and implies that there are no time-dependent effects [27].

Under this condition, the aerodynamic forces are calculated as a sequence of static situations. It is a succession of "*pictures*"of the aircraft at different moments, so the study is performed without regarding the past state (there is no time-dependency). In this case, for the examination of the moving body, the change of both aerodynamic and rate angles are not considered. Also, the wake is modified according to the aircraft instantaneous motion.

An example of it is a constant pull-up. The main forces acting on the aircraft are lift $\boldsymbol{L}$, weight $\boldsymbol{W}$, drag $\boldsymbol{D}$, thrust $\boldsymbol{T}$ (as in steady conditions), and inertial forces. For a general case of quasi-steady aerodynamics, the kinematics values could be the ones in Eq. (1.3).

$$\begin{aligned} \mathbf{V}_0 &= (u, v, w) \\ \mathbf{\Omega} &= (P, Q, R) \end{aligned} \tag{1.3}$$

1.3.3 Unsteady Aerodynamics

Despite the appealing of the quasi-steady assumption due to its simplicity, sometimes is not sufficiently accurate. In case of harmonic or fast maneuvers, more complex aerodynamic analysis must be used in order to predict accurately the dependency of aerodynamic forces and moments on the time content of dynamic motions [27]. The classical approaches to analyze the effects of these motions are Wagner's and Theodorsen's functions. Wagner's function can be used to consider the case of general motion (time domain), while Theodorsen's has main importance to predict aeroelastic effects and the response to continuous turbulence (frequency domain), [27].

When analyzing certain accelerated flights, it is necessary to include in the analysis the wake influence on the aircraft and its own motion history. This is the field of unsteady aerodynamics, an analysis that depends on the history of the motion. It is mandatory to obtain accurate results from sudden flight maneuvers, or short period harmonic motions. An example of it is a diving maneuver, in which the aircraft after a sudden pitch-down descends with a high negative pitch angle. In this case, the most important difference with respect to the quasi-steady approximation is the effect of the wake on the aerodynamic forces and the effects due to the changes of the rotation rates.

The kinematic parameters for general motion (unsteady aerodynamics) analysis are shown in Eq. (1.4). Straight velocity $\boldsymbol{V}$ and angular rate Ω do change with time.

$$\begin{aligned} \mathbf{V}(t) &= (u(t), v(t), w(t)) \\ \mathbf{\Omega} &= (P(t), Q(t), R(t)) \end{aligned} \tag{1.4}$$

Chapter 2

Vortex Lattice Method

"Potential flow is so unphysical that the only fluid to obey its assumptions is dry water"

Richard Feynman, physicist.

2.1 Basics of fluid dynamics

Whenever a flow field is studied there are several ways to classify it. From a classical point of view, a flow field can be either viscous or inviscid, compressible or incompressible, unsteady or steady. While the toughest analysis comes from a fluid that is viscous, compressible and unsteady, the simplest scenario is the one that concerns to flow fields that are steady, incompressible and inviscid [15].

Viscosity, which is also called internal friction, is a fluid's internal resistance to flow. For aerodynamic purposes a flow is considered viscous when it is close to a solid boundary, like the wing of an airplane, where the viscous layer is called boundary layer, Fig. 2.1. It is also viscous the flow in the wake downstream the airplane. Therefore, in aerodynamics, a fluid can be assumed as inviscid when it is outside these areas.

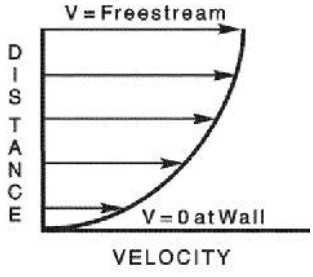

Figure 2.1: Boundary layer velocity profile

A flow with constant density is called incompressible. In contrast, a flow where the density is variable is called compressible [1]. All aeronautical flow fields are compressible, but this is only accounted when the ratio between the local velocity of the fluid and the local speed of sound (Mach number) reaches a certain point.

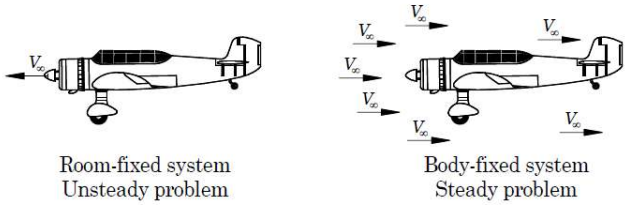

Figure 2.2: Fixed and moving systems of reference, [15].

Every flow field is also time-dependent, but in this case as in the previous, there are some conditions that the fluid must accomplish so this property is not neglected. The election of a reference system has main importance. A body moving relative to a fixed reference system (i.e. Earth) always generates an unsteady flow while the same flow field in a fixed-body reference system can produce a steady flow field [15], see Fig. 2.2. The state and motion of the fluid can be characterized by its velocity, pressure, and temperature. Hence, the flow is steady if all these entities are independent of time in all points of the chosen reference system.

2.1.1 Kinematic concepts

The kinematics of flow fields is geometrically described with concepts such as:

- Pathline: is the path taken by a volume-less fluid particle.
- Streamline: a line in the flow field with the property that the fluid velocity vector is pointing in its tangent direction. If flow is steady, pathlines and streamlines coincide [1].
- Stream tube: real or imaginary tube in the flow field bounded by streamlines.
- Stream tube flow: 1-D approximation in which the velocity, the density, the pressure are constant over the stream tube sections of the coordinate s along the stream tube (and the time).

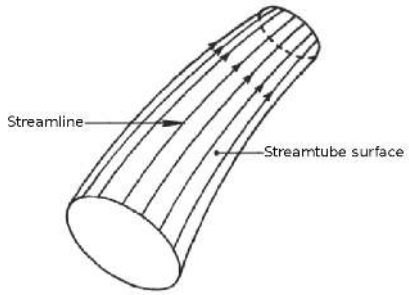

Figure 2.3: Cross section of a stream tube

2.1.2 The Continuity Equation

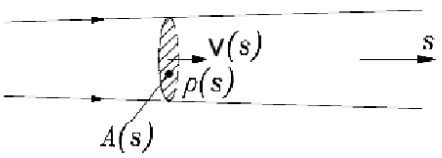

Figure 2.4: Stream tube

In a steady stream tube the mass flow passing through each cross section of it must be the same, Fig. 2.4. This last affirmation is known as the Conservation or Continuity Equation, which is shown in a reduced form in Eq. (2.1) and in its general form in Eq. (2.2).

$$\rho(s)\mathbf{V}(s)A(s) = constant \tag{2.1}$$

where $A(s)$ is the stream tube area in a section determine by the path coordinate s.

$$\frac{\partial \rho}{\partial t} + \nabla(\rho \mathbf{v}) = 0 \tag{2.2}$$

In case of incompressible, steady flow, Eq. (2.2) leads to Eq. (2.3).

$$\nabla \mathbf{v} = \frac{\partial v_x}{\partial x} + \frac{\partial v_y}{\partial y} + \frac{\partial v_z}{\partial z} = 0 \tag{2.3}$$

2.1.3 Bernoulli equation

The Bernoulli equation (2.4) describes the behavior of a fluid moving along a streamline. It is obtained by integrating the Euler equations [25] along a streamline for an inviscid, steady and incompressible flow. Usually, the variation of the potential energy term "$\rho g z$" can be neglected in the air flow [15]. Thus, its physical meaning is clear, there is an inverse relation between the velocity V_s and the pressure p.

$$p + \frac{1}{2}\rho V_s^2 + \rho g z = constant\ along\ the\ streamline \tag{2.4}$$

This equation allows to calculate the forces in many aerodynamic problems. In section 2.4 its unsteady form is posed.

2.2 Potential Flow Theory

In an incompressible and inviscid flow, from the continuity equation there is:

$$\nabla \cdot \mathbf{v} = 0 \tag{2.5}$$

Further, as the flow is irrotational, a velocity potential is introduced:

$$\mathbf{v} = \nabla \phi \tag{2.6}$$

Hence, for an incompressible and irrotational flow, the following equation can be posed:

$$\nabla^2 \phi = 0 \tag{2.7}$$

Eq. (2.7) is known as Laplace equation, which is a second order linear equation. The characteristics associated to linear equations make Laplace's useful for most of aerodynamic problems. It can be applied when the flow satisfies the potential conditions so the velocity potential exists. As a final remark, there are two phenomena that produce vorticity in aeronautics, viscosity and curved shock waves.

2.2.1 Kelvin's circulation theorem

Let C_1 be a fluid curve in an incompressible, inviscid flow field, i.e. a curve frozen in the fluid, Fig. 2.5. The circulation around the curve C is defined as:

$$\Gamma = \oint \vec{v} d\vec{s} \tag{2.8}$$

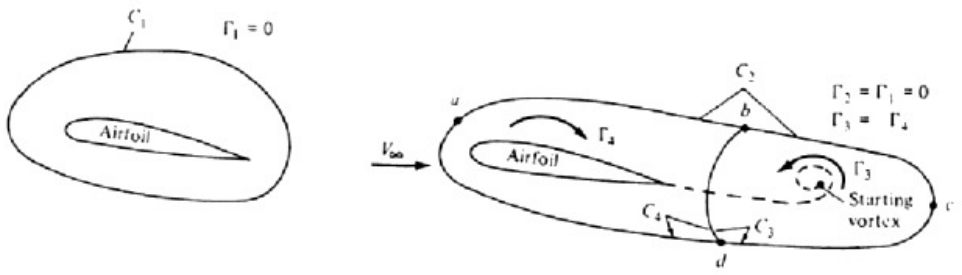

Figure 2.5: Representation of Kelvin's theorem

At some time t, this curves moves in the space. If the flow is inviscid, since C is a fluid curve, from Euler equations [25] it follows Eq. (2.9), a form of angular momentum conservation.

$$\frac{d\Gamma}{dt} = 0 \tag{2.9}$$

Eq. (2.9) is known as Kelvin's circulation theorem. It states that the circulation is constant around any material curve in inviscid flow. For further information, read [16].

2.2.2 Helmholtz theorems

Based on the results of the previous sections, Von Helmholtz stated the following vortex theorems for inviscid flows:

- The strength of a vortex filament is constant along its length.
- A vortex filament cannot start or end in a fluid, it must form a closed path or extend to infinity.
- The fluid that forms a vortex tube continues to form a vortex tube and the strength of the vortex tube remains constant as the tube moves about (hence vortex elements, such as vortex lines, vortex tubes, vortex surfaces etc, will remain vortex elements with time).

2.2.3 Kutta-Joukowsky theorem

A generic aerodynamic force in an incompressible, inviscid, irrotational flow in an unbounded fluid is of magnitude $\rho V_\infty \Gamma$ per unit width, and acts in a direction normal to the free stream [16]. By using vector notation, the previous expression becomes Eq. (2.10), the Kutta-Joukowski theorem.

$$\boldsymbol{l} = \rho \mathbf{V}_\infty \times \mathbf{\Gamma} \tag{2.10}$$

where $\boldsymbol{l}$ is the aerodynamic force per unit width, V_∞ is the free stream velocity and $\mathbf{\Gamma}$ is the circulation around the airfoil in Fig. 2.6. Circulation $\mathbf{\Gamma}$ is positive defined according to right-hand rule.

There are two conclusions that are worthy to highlight from Kutta-Joukowski theorem. The first is that, within the domain of the potential theory, the force over an airfoil is perpendicular to the free stream velocity. The second is that the lift needs of circulation Γ in order to exist. For further information about the derivation of the equation, check [22].

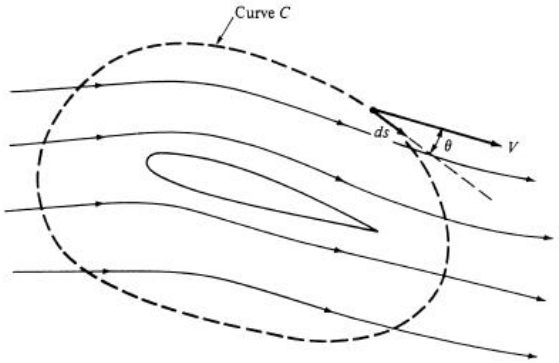

Figure 2.6: Kutta-Joukowski

2.2.4 Boundary conditions

The potential flow theory states some boundary conditions that have to be fulfilled to solve Laplace equation. The first of them requires zero-normal velocity across the body's solid boundary surfaces:

$$(\nabla\phi + \mathbf{V})\mathbf{n} = 0 \ (in\ X,\ Y,\ Z\ coordinates) \tag{2.11}$$

where $\nabla\phi$ is the variation of the velocity potential (or flow disturbance) in $(X,\ Y,\ Z)$ coordinates, $\mathbf{V}$ is the total velocity on the body surface and $\mathbf{n}$ is the normal vector to the surface. The second boundary condition states that the flow disturbance produced by the motion of the lifting body in the fluid has to diminish far from the body. It is posed in Eq. (2.12).

$$\lim_{|\mathbf{R}-\mathbf{R}_0|\to\infty} \nabla\phi = 0 \tag{2.12}$$

where $\mathbf{R}$ is the position of the disturbed flow particle and $\mathbf{R}_0$ is the location of the body.

The Kutta condition (Fig. 2.7) states that the flow must leave the aerofoil at the sharp trailing edge [1]. In inviscid, potential flow, it implies that there must be a stagnation point at the trailing edge. The implementation of the Kutta condition in a mathematical model is done in two main ways:

- The pressure jump over the trailing edge is prescribed to be zero.
- There is a streamline that leaves the aerofoil trailing edge along the bisector to the trailing edge angle δ_{TE} .

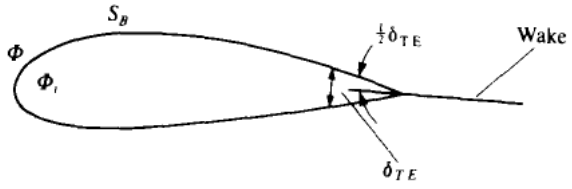

Figure 2.7: Kutta assumption for the wake shape near the trailing edge

2.2.5 Biot-Savart's Law

Find the solution to:

$$\begin{aligned} \nabla \times \mathbf{u} &= \mathbf{w} \\ \nabla \mathbf{u} &= 0 \end{aligned} \tag{2.13}$$

in free space, say $\mathbf{w}$ has compact support.

Since $\mathbf{u}$ is divergence free, we may say

$$\mathbf{u} = \nabla \times \mathbf{A} \tag{2.14}$$

where $\mathbf{A}$ is the vector potential for $\mathbf{u}$. Take the curl again,

$$\nabla \times (\nabla \times \mathbf{A}) = \mathbf{w} \tag{2.15}$$

$$\underset{choose=0}{\nabla\ (\nabla \mathbf{A})}\ - \Delta \mathbf{A} = \mathbf{w} \tag{2.16}$$

Since $\mathbf{w}$ is a curl we have $\nabla \cdot \mathbf{w} = 0$ so our "choice" $\nabla \cdot \mathbf{A} = 0$ is justified. From the Green's function for the Laplace operator in free space there follows:

$$\mathbf{A}(\mathbf{x}) = \frac{1}{4\pi} \int \mathbf{w}(\mathbf{y}) \frac{1}{|\mathbf{x} - \mathbf{y}|} dV \tag{2.17}$$

and finally:

$$\mathbf{u} = \nabla \times \mathbf{A}(\mathbf{x}) = \frac{1}{4\pi} \int \mathbf{w}(\mathbf{y}) \times \nabla \frac{1}{|\mathbf{x} - \mathbf{y}|} dV \tag{2.18}$$

$$\mathbf{u} = \frac{1}{4\pi} \int \mathbf{w}(\mathbf{y}) \times \frac{\mathbf{x} - \mathbf{y}}{|\mathbf{x} - \mathbf{y}|^3} dV \tag{2.19}$$

Eq. (2.19) is the Biot-Savart law. If $\mathbf{w}$ is concentrated to a surface or curve, the integral is changed accordingly.

2.2.6 Horseshoe vortex

For posing an aerodynamic model the first thing to do is to establish the properties that the model have to fulfill [15]. In the present case, these are:

- For a wing generating lift there must be a circulation around each curve encircling any aerofoil section.
- Downstream each wingtip there is a trailing vortex.

A valid model with these properties is the so called horseshoe vortex model, Fig. 2.8. In the following sections other configurations are depicted.

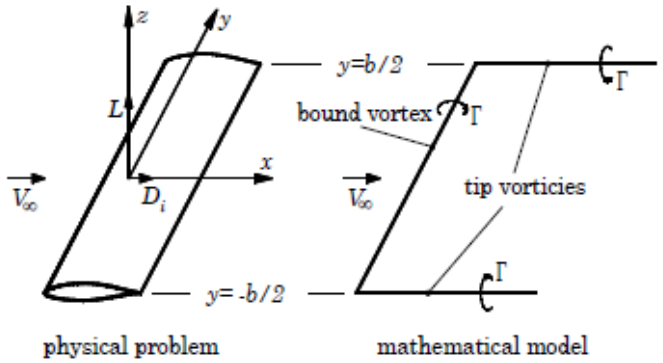

Figure 2.8: Physical problem and mathematical model for a horseshoe vortex, [1].

The horseshoe vortex model consists of a bound vortex and two trailing vortices. There is also a starting vortex parallel to the bound vortex and located downstream of the wing, in the infinity. The

bound vortex replaces the wing and becomes the source of lift through the Kutta-Joukowski law, Eq. (2.10). According to one of the Helmholtz vortex theorems the bound vortex cannot end at the wing tips, so it continues downstream, creating the wake, which is modeled by the trailing vortices. The two half-infinite vortices generate a downsweep along the bound vortex. With the coordinate system in Fig.2.8 this induced downsweep is given by using Biot-Savart law, Eq. (2.19).

2.2.7 Vortex Rings

The vortex rings are a generalization of the horseshoe model. Theoretically, the horseshoe vortex is presented as a vortex ring with trailing segments of infinite length, Fig. 2.9a. However, in practice, it only has three segments while the vortex ring is formed by four straight segments. The bound vortex is forward, the starting one is in the rear position and, linking both of them, there are two trailing vortices, Fig. 2.9b.

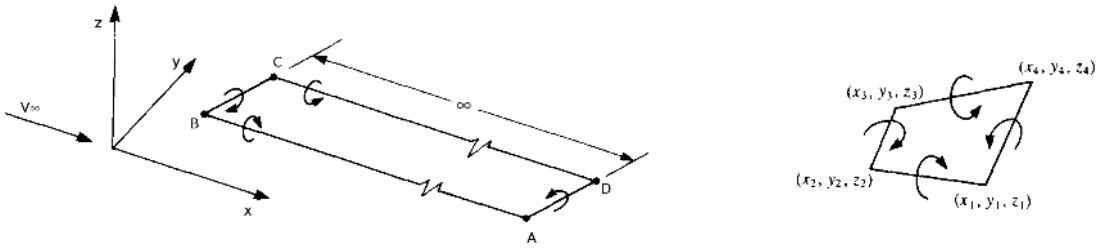

(a) Horseshoe vortex, [1] (b) Vortex ring

Figure 2.9: Vortex ring definition

One advantage of this configuration with respect to horseshoe vortices is that by using vortex rings the zero normal flow condition can be satisfied on the actual wing surface.

2.3 Classical Vortex Lattice Method

The vortex lattice method (VLM) is a potential flow solver based on the lifting line model, [24]. "It represents the wing as a planar surface on which a grid of horseshoe vortices is superimposed" [2]. Although this definition is correct for the classical method, there are several VLM that can modify that statement. In this section, only the classical implementation is described, so the basic horseshoe vortex model is taken into account.

Knowing that vortices represent lift from the Kutta-Joukowski theorem, one approach is to place the vortex and then satisfy the boundary condition of zero normal velocity on the wing surface using the "$1/4 - 3/4$ *rule*"[35]. The procedure is:

1. Divide the planform up into a lattice of quadrilateral panels, and put a horseshoe vortex on each panel.

2. Place the bound vortex of the horseshoe vortex on the 1/4 chord element line of each panel.

3. Place a collocation point on the 3/4 chord point of each panel at the midpoint in the spanwise direction (sometimes the lateral panel centroid location is used).

4. Assume a flat wake in the usual classical method.

5. Determine the strengths of each Γ_n required to satisfy the boundary conditions by solving a system of linear equations.

6. Calculation of the forces and moments by using the Kuttta-Joukowski theorem.

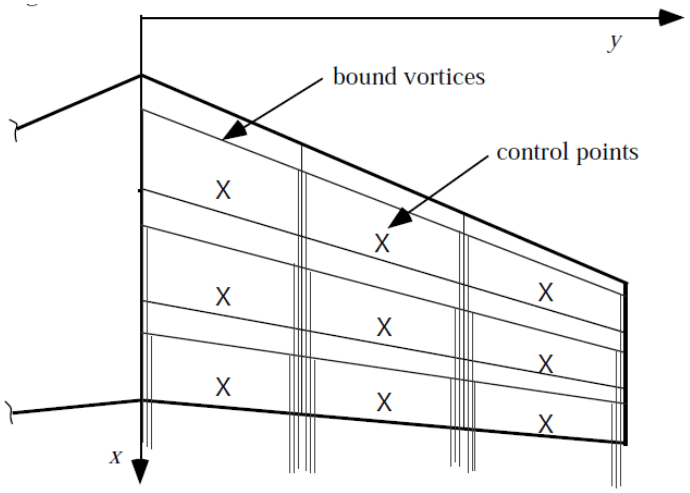

Figure 2.10: Classical vortex-lattice method, [35].

Since the wake is assumed flat, the trailing segments are aligned with the free stream velocity so they are force free. This requirement may produce detachments for a given angle of attack α. However, as small angles of attack are assumed, the wake sheet can be placed in the same plane of the lifting surface.

After the discretization of the wing, the zero normal flow condition has to be satisfied. Eq.(2.11) is defined as an addition of the known free stream speed V_∞ and the unknown velocities induced by the wing bound vortices $\mathbf{v}_b$:

$$(\mathbf{V}_\infty + \mathbf{v}_b) \cdot \mathbf{n} = 0 \tag{2.20}$$

Eq. (2.20) is solved at every collocation point by following a straightforward process. A calculation of the induced velocities starts with Eq. (2.19) for $\mathbf{\Gamma} = 1$, in a horseshoe model. The outcome are the influence coefficients, which are defined in the form of Eq. (2.21).

$$a_{ij} = (u, v, w)_{ij} \cdot \mathbf{n}_i \tag{2.21}$$

where $\mathbf{n}$ is the normal vector to the panel i and $(u, v, w)_{ij}$ are the velocities induced on the collocation point i by the vortex j. From Eqs. (2.20) and (2.20) a linear system of equations (2.22) is set:

$$\begin{bmatrix} a_{11} & a_{12} & \cdots & a_{1N} \\ a_{21} & a_{22} & \cdots & a_{2N} \\ . & & & . \\ . & & & . \\ a_{N1} & a_{N2} & \cdots & a_{NN} \end{bmatrix} \begin{bmatrix} \Gamma_1 \\ \Gamma_2 \\ . \\ . \\ \Gamma_N \end{bmatrix} = \begin{bmatrix} -V_\infty \cdot \mathbf{n}_1 \\ -V_\infty \cdot \mathbf{n}_2 \\ . \\ . \\ -V_\infty \cdot \mathbf{n}_N \end{bmatrix} \tag{2.22}$$

where the circulations Γ_j are the unknowns. After they are calculated, the lift generated by each bound vortex is obtained through Eq.(2.10). In this case, it is posed in a discretized way as Eq.(2.23).

$$\Delta L_i = \rho V_\infty \times \Gamma_i \Delta b_i \tag{2.23}$$

where ΔL_{ij} is the lift of the panel i and Δb_i is the length of the bound vortex of the same panel. To obtain the total lift of the wing, the lifts of all the bound vortices of the wing are summed.

A more sophisticated VLM is Tornado [21], which has been described in section 1.2. It calculates solutions for complex aircraft configurations at steady and quasi-steady flight conditions. However, it lacks an unsteady implementation yet. For more information about this and other vortex lattice solvers, read [21], [34] or [4].

2.4 Unsteady VLM, theoretical background

This section provides a theoretical introduction to the unsteady vortex lattice method. A more detailed explanation of it is given in the next chapter.

Previously, it has been established that a velocity field can be obtained by solving the continuity equation, which does not include time-dependent terms. However, for unsteady conditions these are introduced through the boundary conditions [16]. This statement is the basis of unsteady potential flow theory. Thus, for solving unsteady flows, the same methods as in the steady case apply, with slight modifications. They are, basically, a different treatment of the tangential flow boundary condition, use of the unsteady Bernoulli equation and a more complex wake than in the steady case.

In a dynamic study, the path of an aircraft is determined by the sum of all the forces acting on the aircraft. Since the VLM only concerns about the aerodynamic analysis, the motion of the aircraft follows a prescribed path. Then, two systems of reference are defined, an inertial fixed-to-earth system (X,Y,Z) and a non-inertial fixed-to-body one (x,y,z), Fig. 2.11. The motion of the (x,y,z) system, in relation to the inertial (X,Y,Z), is defined by the instantaneous position of its origin O, Eq. (2.24), and the orientation of the frame, given by the rotation angles, Eq. (2.25).

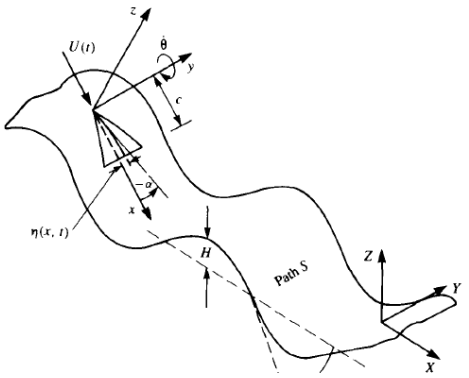

Figure 2.11: Kinematics of the aircraft motion, [16].

$$\mathbf{R}_0(t) = (X_0, Y_0, Z_0) \tag{2.24}$$

$$\mathbf{\Theta}(t) = (\phi, \theta, \psi) \tag{2.25}$$

After inviscid, irrotational, and incompressible flow is assumed, a velocity potential $\Phi(X, Y, Z)$ and, consequently, the Laplace equation Eq. (2.26) can be defined in the inertial coordinate system:

$$\nabla^2\Phi = 0 \ (in \ X, \ Y, \ Z \ coordinates) \tag{2.26}$$

The first boundary condition requires normal velocity across the body's solid boundaries. It is posed as Eq. (2.27).

$$(\nabla\Phi + \mathbf{V})\mathbf{n} = 0 \ (in \ X, \ Y, \ Z \ coordinates) \tag{2.27}$$

Since Eq.(2.26) does not depend directly on time, the time dependency is introduced by Eq.(2.27). The second boundary condition requires that the flow disturbance, due to the body's motion through the fluid, should diminish far from the body:

$$\lim_{|\mathbf{R}-\mathbf{R}_0|\to\infty} \nabla\Phi = 0 \ (for \ any \ t) \tag{2.28}$$

For the unsteady flow Kelvin theorem supplies an additional equation that can be used to determine the stream-wise strength of the vorticity shed into the wake [16]. It states that in the potential flow

region the angular momentum cannot change, so the circulation Γ around the fluid curve enclosing the wing and the wake is conserved.

$$\frac{d\Gamma}{dt} = 0(foranyt) \tag{2.29}$$

The solution of this problem, which becomes time-dependent because of the boundary condition (2.27), is executed in the body-fixed coordinate system. Then, a transformation between the coordinate systems has to be defined:

$$\begin{bmatrix} x \\ y \\ y \end{bmatrix} = f\left(X_0, Y_0, Z_0, \phi, \theta, \psi\right) \begin{bmatrix} X \\ Y \\ Z \end{bmatrix} \tag{2.30}$$

where the left side represent the coordinates $(x,\ y,\ z)$ in the non-inertial coordinate frame and the right side has the transformation matrix $f\left(X_0, Y_0, Z_0, \phi, \theta, \psi\right)$ and the coordinates $(X,\ Y,\ Z)$ in the inertial system. Similarly, the kinematic velocity $\mathbf{V}$ of the lifting surface as viewed from the inertial frame of reference is given by:

$$\mathbf{V} = -\left[\mathbf{V}_0 + \mathbf{v}_{rel} + \Omega \times \mathbf{r}\right] \tag{2.31}$$

Then, if Eq.(2.31) is substituted in Eq.(2.27), it follows:

$$\left(\nabla\Phi - \mathbf{V}_0 + \mathbf{v}_{rel} + \Omega \times \mathbf{r}\right)\mathbf{n} = 0\ (in\ x,\ y,\ z\ coordinates) \tag{2.32}$$

From this equations it is noticed that, for incompressible flow, the instantaneous solution of Eq. (2.26) is independent of time derivatives and, consequently, steady-state techniques can be used for the unsteady problem by substituting the boundary condition at every moment. However, the wake has to be treated differently. Its separation line is dictated by the Kutta condition, and, along trailing edges of lifting surfaces, the velocity has to be finite.

For the wake modeling, additional considerations are taken into account. To obtain the wake strength the simplest solution to this problem is to apply the Kutta condition along the trailing edges of lifting wings.

$$\Gamma_{T.E.} = 0 \tag{2.33}$$

The validity of the assumption depends on the component of the kinematic velocity, normal to the trailing edge, which must be much smaller than the characteristic velocity for Eq. (2.7) to be valid, [16]. Besides, the Kevin condition can be used to calculate the change in the wake circulation:

$$\frac{d\Gamma}{dt} = 0 \tag{2.34}$$

Also, since the trailing edge has a finite angle, a new assumption has to be made to define how the flow is shed in the wake. It is enough to postulate that the wake leaves the wing at the bisector of the trailing edge angle $\delta_{T.E.}/2$, as shown in Fig.2.7

The only equation that has to be defined yet is the unsteady Bernoulli equation. In the inertial frame of reference, from Eq.2.4, it becomes:

$$\frac{p_\infty - p}{\rho} = \frac{(\nabla\Phi)^2}{2} + \frac{\partial\Phi}{\partial t} = \frac{1}{2}\left[\left(\frac{\partial\Phi}{\partial X}\right)^2 + \left(\frac{\partial\Phi}{\partial Y}\right)^2 + \left(\frac{\partial\Phi}{\partial Z}\right)^2\right] + \frac{\partial\Phi}{\partial t} \tag{2.35}$$

where p_∞ is the pressure in the free stream, $\frac{(\nabla\Phi)^2}{2}$ is the gradient of the velocity potential and $\frac{\partial\Phi}{\partial t}$ is the velocity potential time derivative. The last can be obtained in terms of the circulation, establishing the following relations [16]:

$$\Phi^{\pm} = \pm\int \frac{\gamma}{2} dl\ (Integrating\ from\ the\ leading\ edge) \tag{2.36}$$

Since for the vortex model that is used here $\Delta\Phi = \Gamma$, then:

$$\pm \frac{\partial \Phi_{ij}}{\partial t} = \pm \frac{\partial \Gamma_{ij}}{2\partial t} \tag{2.37}$$

Chapter 3

ABSOLUT, the Computational Method

"Aeronautics was neither an industry nor a science. It was a miracle."

Igor Sikorsky, helicopter's inventor.

ABSOLUT is a potential flow solver, developed in MATLAB environment, which is based on Hedring, a Fortran algorithm developed by Sven Hedman [10], and Tornado [32]. The main differences from Hedring consist of a more complex geometry discretization and a general motion definition.

With respect to Tornado, the main divergence is that the present code is an unsteady vortex lattice method and employs, instead of vortex slings, vortex rings. Its solution method concerns the time domain so it follows an iterative process divided in time-steps. The wing (or wings), which has been divided in panels, starts its motion with no wake at first. However, in the following time steps the vortex rings of the trailing panels are shed at the rate of one row of rings per step, Fig 3.1. This sequence is used for any prescribed motion of the lifting surface.

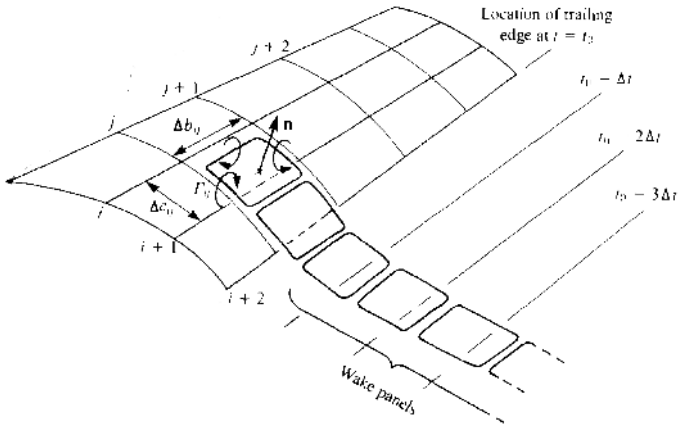

Figure 3.1: Unsteady Vortex lattice method for vortex rings

The forces are calculated in the same way as in the classical vortex lattice method, described in the previous chapter. First, a linear system of equations is solved in order to obtain the circulation of the vortex rings. Then, the forces are calculated by means of the Kutta-Joukowski theorem. Nevertheless, in this case there are certain modifications that introduce the time-dependence. Eq. (2.22) is modified so it takes account the rotation rates of the aircraft and the velocity induced by the wake. Besides, a new

term is added to the Kutta-Joukowski equation in order to include the lag influence.

The following sections of this chapter aim to describe in depth relevant features of the computational method explained here.

3.1 Code Structure

As it is shown in the flow chart of the code, Fig. 3.2, the program has three main divisions:

- The **preprocessor** manages input variables such as the geometric data and the prescribed motion of the aircraft configuration. Besides, it defines the geometry of the lifting surfaces and discretizes them. The final task of this step is the generation of the lattice mesh according to the geometry and the type of motion of the aircraft.

- In the **processor** the solver calculates the forces and moments under steady and unsteady aerodynamic conditions. It also models the wake shape.

- The **postprocessor** calculates the stability derivatives and generates the plots of the solutions obtained from the solver.

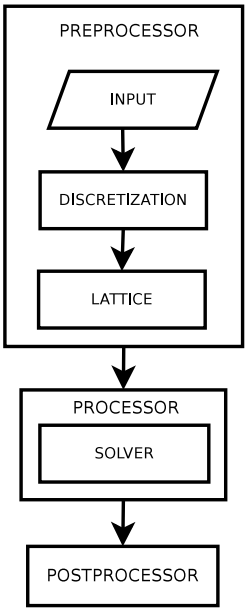

Figure 3.2: Flow chart of the code

For a functional description of the different files and variables of the code, check appendix A.

3.2 Preprocessor

After obtaining the inputs and adjusting them for the next step, the Preprocessor starts an iterative process, Fig. 3.3. The lifting surfaces are defined, discretized and meshed, partition by partition. The coordinate systems are the same as in Tornado and in [16]. The origin O is usually placed in the center of gravity, the axis OZ points downward, the OX axis backward in the direction of the mean aerodynamic chord and the OY axis forms, together with the other two, a right handed coordinate frame.

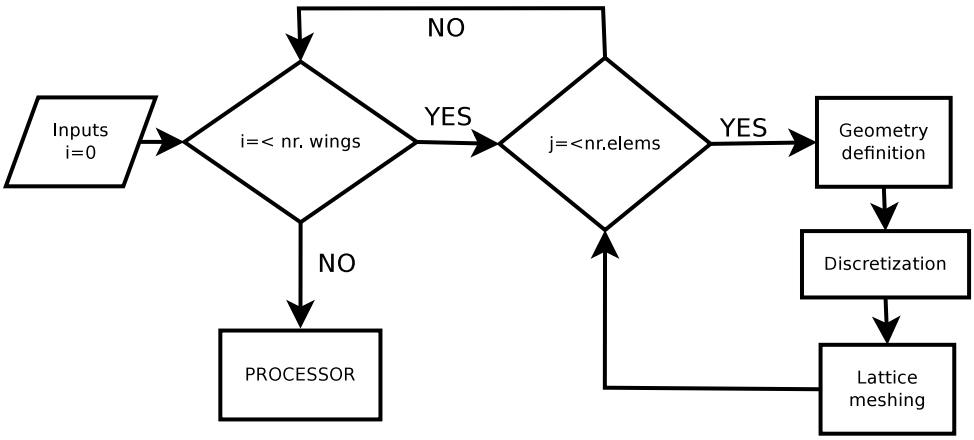

Figure 3.3: Flow chart of the Preprocessor

3.2.1 Inputs

As in Tornado, the user is able to set the parameters that define the geometry of the wing configuration together with the flight characteristics. The only difference is that in this extension there are some more flight options. Since this solver works for both unsteady and steady cases, there is the possibility of choosing one of them. The steady alternative of the code works, basically, as Tornado. However, in the unsteady choice new variables appear. There is the chance of selecting a harmonic motion for the aircraft and of specifying unsteady deflections of the control surfaces (with the harmonic option too). Consequently, the aerodynamic analysis of moving control surfaces is also possible.

3.2.2 Discretization

The discretization of the lift surfaces is performed as in Tornado [21]. Thus, to define the geometry of the wings, they are divided in multiple partitions or segments, Fig. 3.4.

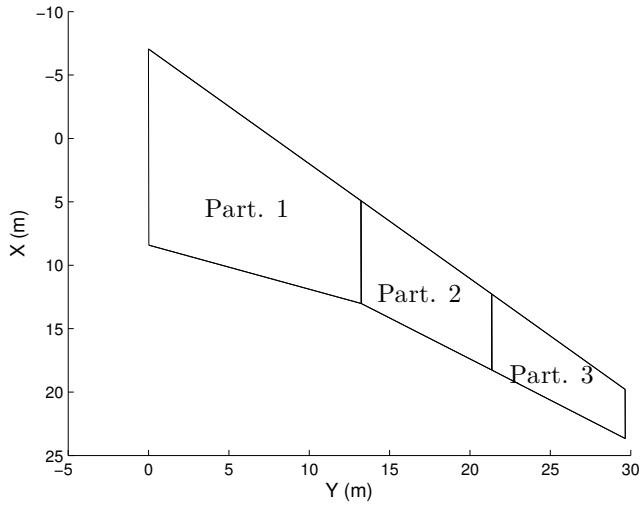

Figure 3.4: Planform view of the main semi-wing of a B-747 model

A partition of a wing is a quadrilateral element that is defined by the coordinates of its four corners. Each segment has the same properties of a whole wing, which means that it has sweep angle Λ, taper ratio λ, dihedral angle Γ, as well as twist θ.

The coordinates of a partition are specified by Tornado and ABSOLUT similarly.

- First quad of the wing: reference point is the apex of the wing. From the coordinate established in the geometry inputs, in case there is torsion in this wing section, a rotation is performed in Y-direction, taken as rotation center the quarter chord of the wing.

- Other quads of the wing: reference point is the second vertex of the previous partition. Then, the rest of the segment is rotated as before.

- Flap partition: reference point is the fourth vertex of the main partition.

The process to obtain the final position of the partition is described by Eqs. (3.1), (3.2, (3.3)), (3.4, (3.5)) and (3.6). The first four define the displacement of the partition in relation to the quarter chord point. Therefore, rotations about Y axis are predominant. The subscripts *in* and *out* refer to the inboard and outboard side of the partition respectively.

$$\Delta x = \begin{bmatrix} (1 - cos(\theta_{in})) \cdot cos(\Lambda) \\ (1 - cos(\theta_{out})) \cdot cos(\Lambda) \\ (1 - cos(\theta_{out})) \cdot cos(\Lambda) \\ (1 - cos(\theta_{in})) \cdot cos(\Lambda) \end{bmatrix} \tag{3.1}$$

$$\Delta y = \begin{bmatrix} -sin(\theta_{in}) \cdot sin(\Gamma) \cdot cos(\Lambda) \\ -sin(\theta_{out}) \cdot sin(\Gamma) \cdot cos(\Lambda) \\ -sin(\theta_{out}) \cdot sin(\Gamma) \cdot cos(\Lambda) \\ sin(\theta_{in}) \cdot -sin(\Gamma) \cdot cos(\Lambda) \end{bmatrix} \tag{3.2}$$

$$\Delta z = \begin{bmatrix} sin(\theta_{in}) \cdot cos(\Gamma) \\ sin(\theta_{out}) \cdot cos(\Gamma) \\ sin(\theta_{out}) \cdot cos(\Gamma) \\ sin(\theta_{in}) \cdot cos(\Gamma) \end{bmatrix} \tag{3.3}$$

$$\mathbf{C} = \begin{bmatrix} \Delta x \\ \Delta y \\ \Delta z \end{bmatrix} \tag{3.4}$$

Eq (3.5) prescribes, mainly, rotations around X and Z axis,

$$\mathbf{B} = \begin{bmatrix} 0 & b \cdot tan(\Lambda) & b \cdot tan(\Lambda) + \lambda \cdot cr & cr \\ 0 & b \cdot cos(\Gamma) & b \cdot cos(\Gamma) & 0 \\ 0 & b \cdot sin(\Gamma) & b \cdot sin(\Gamma) & 0 \end{bmatrix} \tag{3.5}$$

In Eq. (3.6) all rotations are set together:

$$\begin{bmatrix} x \\ y \\ z \end{bmatrix} = \mathbf{B} \cdot \mathbf{c_{rot}} + \mathbf{C} + \mathbf{c_{ref}} \tag{3.6}$$

where c_{rot} is the distance from the leading edge to the quarter chord line of the wing and $\mathbf{c_{ref}}$ is the reference coordinate for the partition. The discretization of the wing in several panels is done in the same way as Tornado, [21]. An example is given in Fig. 3.5 where a X31 VLM model has been divided into panels.

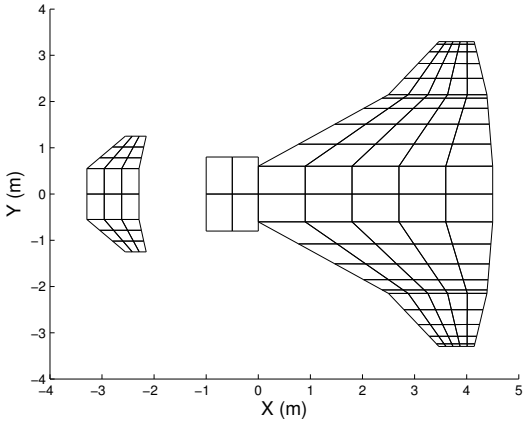

Figure 3.5: Planform view of X31 VLM model discretized

3.2.3 Lattice meshing

Once the aircraft geometry is discretized, the meshing of it is performed by using the vortex rings concept, section 2.2.7. As explained in chapter 2, the boundary conditions to solve the Laplace equation (2.7) must be fulfilled. Consequently, the vortex rings are placed according to classical VLM rules. The bound vortex is located at the quarter chord line of each panel, while the rear segment is at a distance of the panel of a quarter chord of it. The trailing segments link the first two in the X-direction.

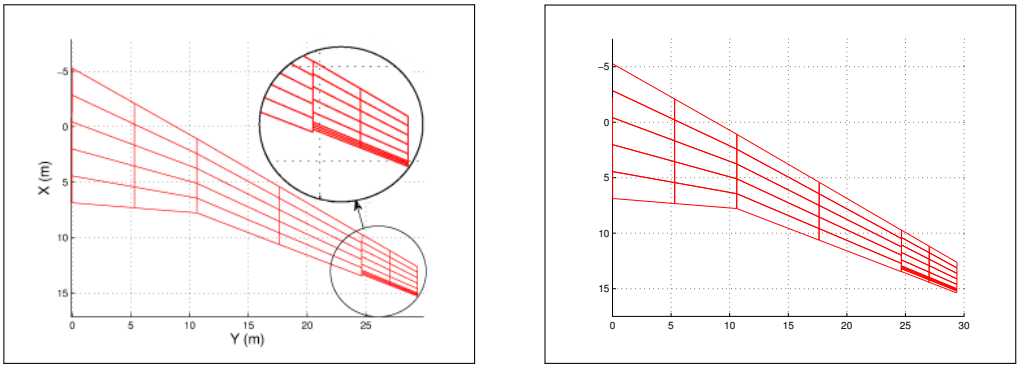

(a) Flap with discontinuity (b) Present meshing

Figure 3.6: Lattice meshing for steady conditions

Trailing edge panels involve a special situation, whether the wing is analyzed in steady or unsteady situation. For the most simple case, the wing does not have any control surface and it is studied under steady conditions. The starting segment of the ring is located as previously, one quarter chord far from the trailing edge. However, if the wing has control surfaces a discontinuity appears in the lattice, Fig. 3.6a. To fix this problem, it has been established that the rear vortex segments of the trailing edge must be a chord length far from the bound vortex segments of the leading edge in each wing section, Fig. 3.6b. For an aircraft studied in unsteady flow conditions, the distance from the rear vortex to the trailing edge panel Δx is obtained by Eq. (3.7).

$$\Delta x = KV_\infty \Delta t \tag{3.7}$$

where V_∞ is the free stream velocity, Δt is the time step between two calculations and K is a constant that usually is taken between $0.2 - 0.3$ [16].

3.2.4 Airfoil

A more realistic approach than the classical VLM is to adjust the wing geometry to the airfoil in each wing section. As only surfaces are accounted for this method, the wing airfoil geometry is approximated by the mean camber line.

The generation of camber lines in each partition starts with the airfoils chosen for the inboard and outboard sides of it. In case the segment has the same airfoils in both kinks, every section of the partition has the same camber line. However, if the inboard airfoil is different from the outboard one, the profiles in between are calculated through linear interpolation of the values of the main two, adjusted by the relative distance to each side. The last situation is known as aerodynamic twist.

Despite Tornado defines the normals of each panel as if they were placed in each airfoil, in fact it does not displace the real panel to the mean camber line. It is impossible due to the characteristics of the horseshoe (sling) vortices. However, in ABSOLUT vortex rings are actually placed on the mean camber line. In Fig. 3.7, blue segments represent the orientation of the vortex sling panels (Tornado) while the red segments do the same for the position of the vortex rings panels (ABSOLUT). The black curve is meant to be the mean camber line and the arrows the normal direction in each division of it.

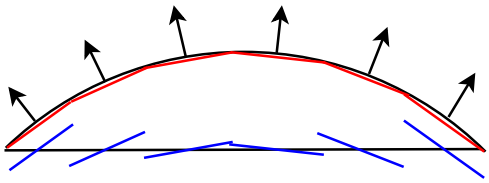

Figure 3.7: Profile definition

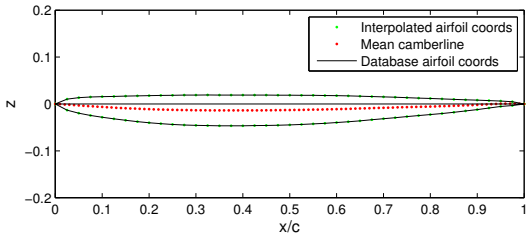

Figure 3.8: Coordinates of X31-W1 airfoil

When obtaining the mean camber line, three cases are possible. In the first one, the discrete coordinates of the airfoil are obtained from a database, and several points are calculated by interpolating at the upper and lower sides. Then, the mean camber line is obtained, Fig. 3.8. Also, it can occur that the airfoil is not in the database. If it is a 4-series NACA profile, the mean camber is generated by well-known formulas, which can be found in [29]. In the last case, the airfoil is not found in the database and it is not a NACA profile, so it is assumed a flat plate (NACA 0012). Fig. 3.9 shows how the shape of a wing partition changes due to the addition of camber to it. The black mesh represents the partition prior to the camber addition. The red one, on the contrary, is the segment when the camber has already been added.

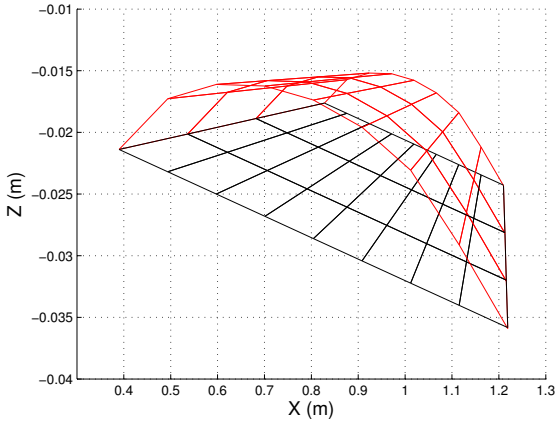

Figure 3.9: Wing's partition of the TCR-C15 VLM model

The addition of the real camber, not only the normal directions, has no main importance for the calculation of the different forces, since they only concern about the orientation of the panel.

3.3 Processor, the solver

The potential flow solver follows the chart shown in Fig. 3.10, based on one from [16]. It performs a certain number of iterations that is established by the input variables. When iteration number is larger than the number of steps, the loop stops and the postprocessor starts.

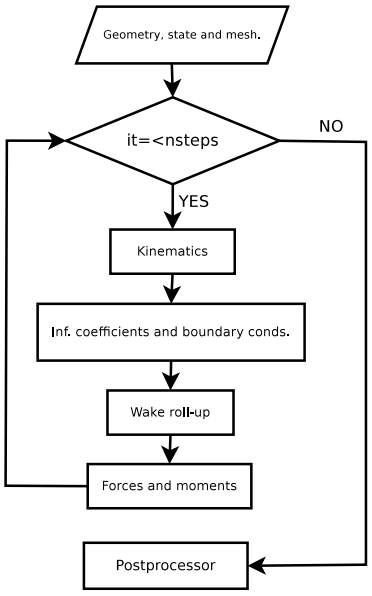

Figure 3.10: Flow chart of solver

For the steady version the solver flow chart looks almost the same, apart from the lack of some steps. In the steady version the number of steps is one, so the loop disappears. Also, since the analysis is steady or quasi-steady both the kinematics and the wake roll-up steps also vanish.

3.3.1 Kinematics

As it has been explained in section 2.4, for the unsteady case, two systems of reference are defined, one fixed to Earth (inertial) and the other fixed to the aircraft body (non-inertial). For the inertial system

of reference it is assumed flat Earth. In Fig. 3.11 both systems are shown according to CEASIOM definitions [8]. In the fixed Earth axes (O_1, X_1, y_1, z_1), z axis points downwards, while x and y axes conform a right-handed coordinate system. In the body axes system the origin is a constant point of the body (usually 1/4 Mean Aerodynamic Chord), axis OX is parallel to the MAC and pointed forward, axis OZ is pointed down, and axis OY is pointed to the right wing.

In $t = 0$ body and Earth coordinate systems are aligned. However, for next time steps a transition coordinate of reference (O, X_g, y_g, z_g) is generated. It is parallel to the Earth system but its origin is attached to the one of the body fixed frame.

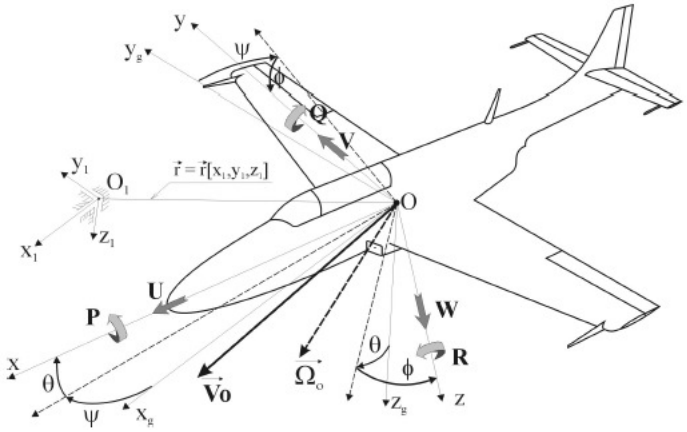

Figure 3.11: Wind's reference system according to CEASIOM definitions [8]

Eq. (3.9) is the rotation matrix between the transition (O, X_g, y_g, z_g) and the body-fixed system (O, x, y, z) velocities,[8]. The roll angle ϕ, the pitch θ and the yaw ψ define the rotations performed about x_g, y_g and z_g respectively in the same order in which they have been named. They are quasi-Euler angles.

$$\begin{bmatrix} \dot{x} \\ \dot{y} \\ \dot{z} \end{bmatrix} = A_V \begin{bmatrix} U \\ V \\ W \end{bmatrix} \tag{3.8}$$

where $(\dot{x}, \dot{y}, \dot{z})$ are the linear velocities in the gravity inertial system and (U, V, W) are the velocities in the body system of reference

$$A_V = \begin{bmatrix} cos\theta cos\psi & cos\psi sin\theta sin\phi - cos\phi sin\psi & sin\phi sin\psi + sin\theta cos\phi cos\psi \\ cos\theta sin\psi & sin\psi sin\theta sin\phi + cos\phi cos\psi & sin\theta cos\phi sin\psi - cos\psi sin\phi \\ -sin\theta & sin\phi cos\theta & cos\phi cos\theta \end{bmatrix} \tag{3.9}$$

Eq. (3.10) describes the influence of the rate velocities in the transformation between coordinate frames. The deformation terms are added in Eq. (3.11).

$$\begin{bmatrix} U_5 \\ V_5 \\ W_5 \end{bmatrix} = \begin{bmatrix} -\dot{\theta}z + \dot{\psi}y \\ -\dot{\psi}x + \dot{\phi}z \\ -\dot{\phi}y + \dot{\theta}x \end{bmatrix} \tag{3.10}$$

$$\begin{bmatrix} U_6 \\ V_6 \\ W_6 \end{bmatrix} = \begin{bmatrix} 0 \\ 0 \\ -\frac{\delta\eta}{\delta t} \end{bmatrix} \tag{3.11}$$

where $-\frac{\delta\eta}{\delta t}$ is the deformation change in time of the lifting surface. ABSOLUT updates the position of the aircraft in the inertial frame of reference in each time step, given the the prescribed path and velocities for the aircraft. In case the aircraft has control surfaces, as ailerons, rudder or elevators, a new term is added.

3.3.2 Influence coefficients and boundary conditions

To fulfill the zero-normal velocity across the body's solid boundary, Eq. (3.13), first the velocities induced by aircraft rings on their collocation points are calculated by using Biot-Savart equation (2.19) with circulation set to $\Gamma = 1$. The velocity induced in a collocation point i by a vortex ring j is the result of adding of the four vortex segments of the ring. These induced velocities with unitary circulation become influence coefficients a_{ij} of Eq. (3.13) in the following equation:

$$a_{ij} = \omega_{ij} \cdot \mathbf{n}_i \tag{3.12}$$

where ω_{ij} is the velocity induced in the collocation point i by the vortex ring j and $\mathbf{n}_i$ is vector normal to the surface of the panel i. For the case of a rigid aircraft without moving parts (control surfaces or deformations), the influence coefficients remain constant in time. The reason is that the Biot-Savart only depends on the relative coordinates of the vortex rings with respect to the collocation points. From Eq. (2.22) it follows Eq. 3.13. They differ in the time dependence so Eq. 3.13 right hand-side is modified in each time step.

$$\begin{bmatrix} a_{11} & a_{12} & \cdots & a_{1N} \\ a_{21} & a_{22} & \cdots & a_{2N} \\ . & & & . \\ . & & & . \\ a_{N1} & a_{N2} & \cdots & a_{NN} \end{bmatrix} \begin{bmatrix} \Gamma_1 \\ \Gamma_2 \\ . \\ . \\ \Gamma_N \end{bmatrix} = \begin{bmatrix} RHS_1 \\ RHS_2 \\ . \\ . \\ RHS_N \end{bmatrix} \tag{3.13}$$

The right hand-side of Eq.(3.13) is calculated in Eq. (3.14), $\mathbf{V}_w(t) = (u_w, v_w, w_w)$ is the inwash produced by the wake in any of the collocation points, and $\mathbf{V}(t) = (u(t), v(t), w(t))$ are the velocities obtained from Eq. (2.31) in the non-inertial system of reference.

$$RHS_k = -[U(t) + u_w, V(t) + v_w, W(t) + w_w,]_k \cdot \vec{n}_k \tag{3.14}$$

Once the circulations $\mathbf{\Gamma}$ of every vortex ring are obtained, the velocities induced in each bound segment have also to be calculated. Therefore, the same process is followed, with the exception of that the circulation has already been obtained, so the velocities are gathered as in Eq. (3.15).

$$V_{bv} = \mathbf{V}(t)_{bv} + \mathbf{V}_w(t)|_{bv} + \Gamma \cdot \mathbf{a}_{ij}|_{bv} \tag{3.15}$$

where bv subscript denotes that the velocities are obtained in the bound vortex segment of the vortex rings.

3.3.3 Forces and Moments

In the steady case, forces are calculated as in Tornado. The only exception is that, since vortex rings are treated here, instead of horseshoe vortices, the bound vortex strength of each ring is calculated as the difference between the total circulation of it and the circulation of the precedent vortex ring. An explanation of how horseshoe vortices and vortex rings are related is given in [23].

In order to calculate the forces in the unsteady case Eq. (2.35) has to be discretized, becoming Eq. (3.18)

$$\Delta p_{ij}|_{st} = \rho(\mathbf{\Gamma}_{ij} - \mathbf{\Gamma}_{i-1,j}) \times \mathbf{V}_{bv} \tag{3.16}$$

$$\begin{aligned} \Delta p_{ij}|_{un} &= \frac{\mathbf{\Sigma}_t - \mathbf{\Sigma}_{t-1}}{\Delta t} \\ where\ \mathbf{\Sigma} &= \frac{\mathbf{\Gamma}_{ij} - \mathbf{\Gamma}_{i-1,j}}{2} + \mathbf{\Gamma}_{i-1,j} \end{aligned} \tag{3.17}$$

$$\Delta p_{ij} = \Delta p_{ij}|_{st} + \Delta p_{ij}|_{un} \tag{3.18}$$

where the subscript t means time.

$$\Delta F = -(\Delta p \Delta S)_{ij} n_{ij} \tag{3.19}$$

$$\Delta m = \Delta \vec{r} \times \Delta \vec{F} \tag{3.20}$$

3.3.4 Stability derivatives

The dynamic derivatives are obtained by using expansion series of MacLaurent. That is a common approach in linear aerodynamics. An example is given in Eq (3.21), where the dependency of the lift forces on the different parameters of flight is described.

$$C_L(t) = C_{L0} + C_{L\alpha}\alpha(t) + C_{Lq}q(t) + C_{L\dot{\alpha}}\dot{\alpha}(t) \tag{3.21}$$

where C_L is the lift coefficient and the different subscripts state the variable of which it is dependent. The calculation of the different components of Eq. (3.21) is handle depending on the subscript. C_{L0} and $C_{L\alpha}$ can be calculated under the steady assumption; the first is a constant of the aircraft while the other depends on a steady variable, the angle of attack. Together, they form the steady or real part of the lift coefficient. In C_{Lq} case, it can be obtained by using the quasi-steady analysis of the aircraft motion. However, $C_{L\dot{\alpha}}$ is the lift coefficient dependent on rate of change of the angle of attack. It depends on the wake, so it can only be studied under unsteady conditions. C_{Lq} and $C_{L\dot{\alpha}}$ are the unsteady or imaginary part of the lift. To calculate $C_{L\dot{\alpha}}$, Eq. (3.22) is divided in its imaginary and its real part. Then, it is used Eq. (3.22):

$$C_{L\dot{\alpha}} = \frac{1}{k \cdot \Delta\alpha}\left(Im(\bar{C}_L) - C_{Lq}\hat{q}(t)\right) \tag{3.22}$$

where k is the reduced frequency of the motion, $Im(\bar{C}_L)$ is the imaginary part of the mean value of $C_L(t)$, $\Delta\alpha$ is the amplitude of the motion and $\hat{q}(t)$ is the nondimensional pitch rate according to [8]. For more information about how the rest of derivatives are calculated, read [18] and [19].

3.3.5 Wake treatment

There are different procedures to treat the wake released from the aircraft in a vortex lattice method. For the steady case, the wake is assumed to be aligned with the free stream and to extend to the infinity. It is modeled as a sum of vortex rings with their trailing segments at distance of $60 \cdot b_{ref}$ from the trailing edge of the wing so its effects are likely neglected, Fig. 3.12.

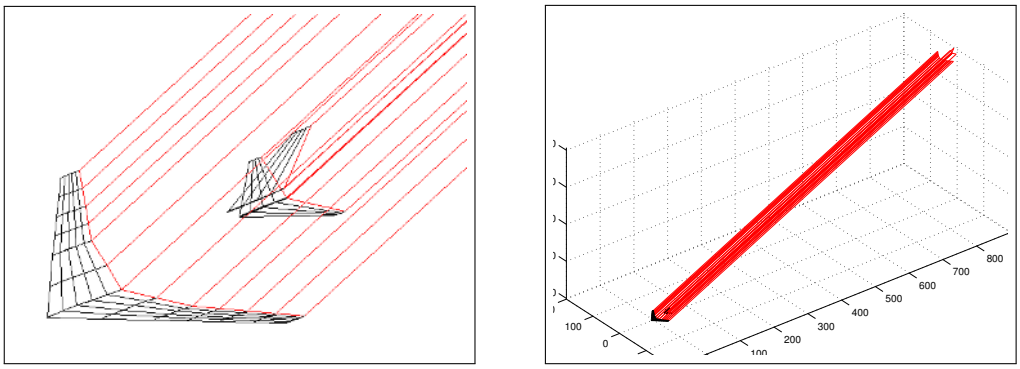

(a) Detail B747 lattice (b) B747 steady wake

Figure 3.12: Flat wake for steady case, $\alpha = 25°$.

For unsteady conditions, as it is explained at the beginning of the chapter, the trailing edge vortex rings are shed in the wake each time step. The strength of these vortex rings is assumed to be constant and equal to the circulation they had on the wing. To fulfill this requirement, each vortex ring of the wake can be treated as a rigid body with constant direction in the space. However the rigid rings' wake has a drawback in its behavior. It is too unstable, and so they are the solutions obtained with such model. Hence, it becomes necessary to smooth the wake behavior in order to stabilize it. The method to achieve it is explained in section (3.3.6).

On the other hand, other type of wake can be modeled. In this one, the wake vortex rings move according to the local velocity in its vortex corners, so they are deformable. In case of a strong wake roll-up,

the size of the wake vortex ring can increase. Apart from the cited deformation, the wake rings suffer a certain torsion in its edges, , and so a change in orientation. These effects, are against the conservation of angular momentum, but the present method presumes them small enough to be neglected, [16].

In Figs. 3.13 and 3.14 the rigid and the deformable vortex rings models are respectively shown. In both plots, a flat plate of aspect ratio $AR = 8$ has been set suddenly in a constant forward speed at an angle of attack $\alpha = 5°$. Due to its instability, the wake in Fig. 3.13 has been smoothed, so it does not perform any roll-up. This, however, can be appreciated in Fig. 3.14. Consequently, the deformable wake has been chosen, since it is more realistic, as the wake model of the present code.

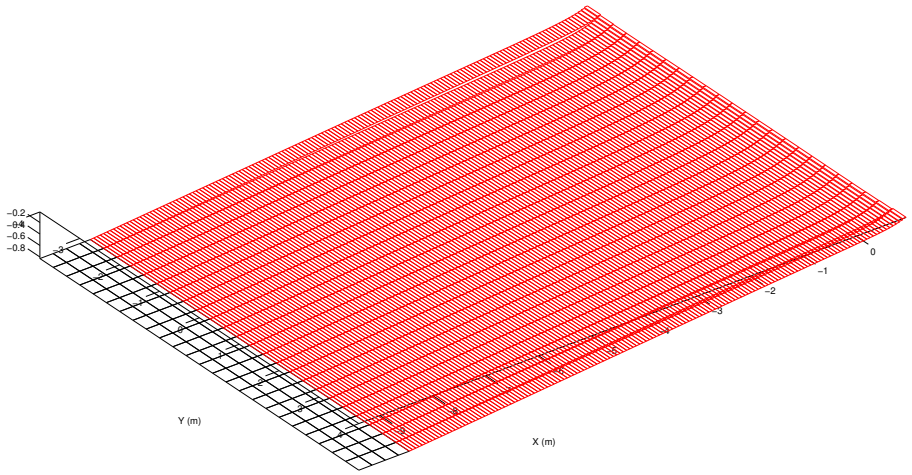

Figure 3.13: Rigid rings' wake after a sudden acceleration of a flat plate with $k = 3$, see section 3.3.6.

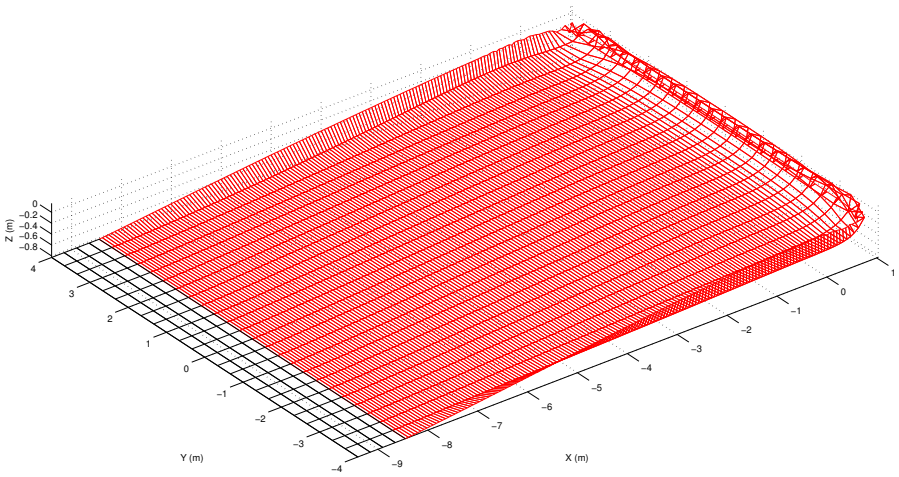

Figure 3.14: Deformable rings' wake after a sudden acceleration of a flat plate with $k = 0$.

For the selected wake, the local stream velocity is the resultant of the velocities induced at each vortex ring corner by the wing and wake itself, and it is measured in the inertial frame of reference (O_1, X_1, y_1, z_1) [16]. To calculate the motion of the vortex rings, the induced velocity $(u, v, w)_t$ is updated at each time step. Then, the vortex elements are displaced by using Eq. 3.23.

$$(\Delta X, \Delta y, \Delta z)_t = (u, v, w)_t \Delta t \tag{3.23}$$

where $(\Delta X, \Delta y, \Delta z)_t$ is the displacement of a certain vortex ring corner due to a velocity $(u, v, w)_t$ over a time Δt.

3.3.6 Singularities in the solution

Cut-off method

Though Biot-Savart equation is valid for most of the situations, there are certain cases in which it calculates unrealistic induced velocities. An example arises when the projection of one of the straight vortex segments intersects with the point in which the velocity is calculated. Instead of a zero induced velocity (reality), the resultant of Eq. (2.19) becomes singular because the minimum distance to the segment is $h = \frac{|\boldsymbol{r}_1 \times \boldsymbol{r}_2|^2}{\boldsymbol{r}_0} = 0$. A discrete form of the Biot-Savart law is Eq. (3.24).

$$\boldsymbol{\omega}_{1,2} = \frac{\boldsymbol{\Gamma}}{4\pi} \frac{\boldsymbol{r}_1 \times \boldsymbol{r}_2}{|\boldsymbol{r}_1 \times \boldsymbol{r}_2|^2} \boldsymbol{r}_0 \cdot \left(\frac{\boldsymbol{r}_1}{r_1} - \frac{\boldsymbol{r}_2}{r_2} \right) \tag{3.24}$$

In the described case a simple approach is chosen. Whenever at a collocation point is a distance inferior to 10^{-8} m from the vortex segment, the induced velocity is set to zero, the so called cut-off method. This is valid for steady conditions as well as for unsteady calculations of single wings. Nevertheless, whenever there is interaction between the wake and downstream surfaces another solution is necessary.

Vortex core size

Whenever the wake interacts with a wing surface, it produces disturbances that can cause its own collapse and instabilities in the forces calculation. To correct the numerical effect, a core size ϵ has been set in Eq. (3.24), which leads to Eq. (3.25). As it is stated in Eq. (3.26), the core size of each vortex ring is established as the maximum length of each panel. Its main effect is to smooth the wake changes and to eliminate the instabilities in the results.

In ABSOLUT, k (see Eq. (3.25)) is a factor that helps to adapt the core size to different aircraft geometries. It is divided in two different constants, k_{wake} and k_{wing}, which depends on the location of the vortex segment. If this is in the wing, it only affects the wake motion and the factor is named k_{wing}. In case the segment is part of a wake vortex ring, the size of the core influences both the wake motion and the wing, and the parameter is called k_{wake}.

An important drawback of this procedure arises whenever the factor k is set too large. A consequence is that wake slows its motion and it even becomes "frozen" in time. For conventional configurations, $k_{wake} = 0$ and $k_{wing} = 0.1$ have reported satisfactory results, while for an aircraft with canard, this parameters rise to $k_{wake} = 0.5$ and $k_{wing} = 1$. A brief description of how the size of the vortex core is obtained can be found in section 5.2.2.

$$\boldsymbol{q}_{1,2} = \frac{\boldsymbol{\Gamma}}{4\pi} \frac{\boldsymbol{r}_1 \times \boldsymbol{r}_2}{(|\boldsymbol{r}_1 \times \boldsymbol{r}_2| + k\epsilon \cdot r_0)^2} \boldsymbol{r}_0 \cdot \left(\frac{\boldsymbol{r}_1}{r_1} - \frac{\boldsymbol{r}_2}{r_2} \right) \tag{3.25}$$

$$\epsilon \simeq max(\Delta b, \Delta c) \tag{3.26}$$

where Δb is the panel span and Δc is the panel chord length.

Chapter 4

Code Validation

> The logic of validation allows us to move between the two limits of dogmatism and skepticism.
>
> Paul Ricoeur, philosopher

The first cases that have been used to validate the program are the ones from Hedring, [10]. It certifies the goodness of the solutions by comparing its results with the ones given in [26] and [16]. All of them are run for flat plates with simple geometries.

4.1 Deflected Flap

The first case tests a wing under steady conditions. A tapered flapped flat plate has been chosen. The wing is swept back $\Lambda = 35°$ in its quarter chord line, and it has an aspect ratio of 4. The flaps deflects symmetrically an angle $\delta = 5.73°$. For the simulation the wing has been divided into 10 panels in chordwise direction and 16 in spanwise direction. It is compared with experimental results from [17] and computational results from Hedring [10]. The velocity is set to $V = 10\ m/s$.

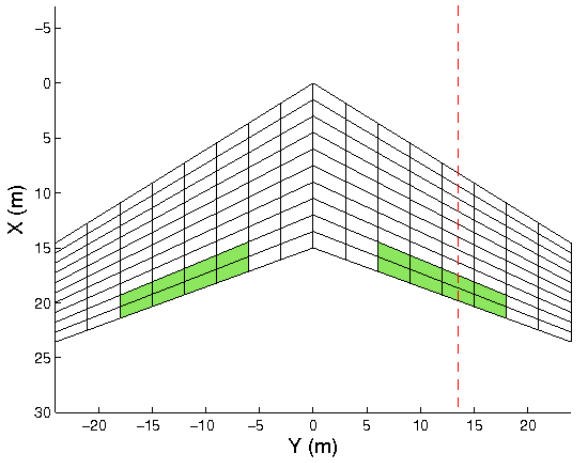

Figure 4.1: Flat plate wing with swept back $\Lambda = 35°$

A planform view of the wing can be seen in Fig. 4.1. The colored panels represent the flaps. The dashed line indicates in which section the pressure distribution has been calculated in Fig. 4.2. This figure shows the pressure distribution in the cited section of the wing when the flap is deflected. It is appreciated that the three set of results have the same tendency. After a smooth fall of the pressure, it suffers a sharp increase due to the flap deflection. Then, it goes down to match the Kutta condition ($p = 0$) at the trailing

edge of the wing. However, there are differences in the values obtained. The experimental pressure is lower than the computational one in almost every point of the chord. It also starts its growth before the two lines. The solvers obtained almost the exact the same results in every part but for the top of the curve, where Hedring calculates a higher pressure. Nevertheless, both computational calculations seem to agree almost perfectly.

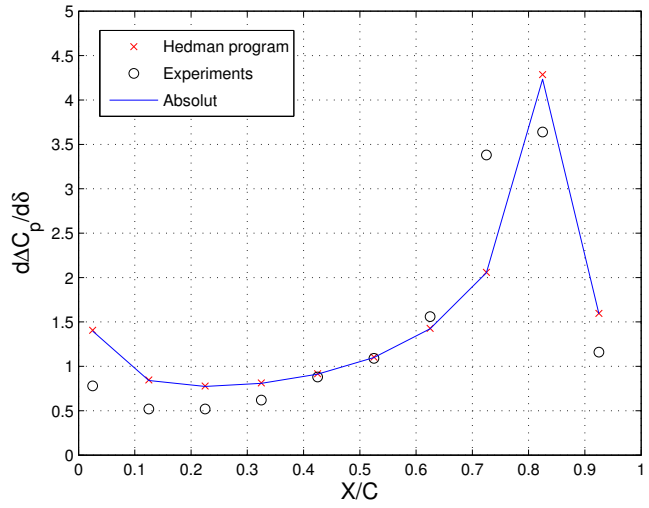

Figure 4.2: Pressure distribution for a deflection of 5.73°

4.2 Sudden acceleration

Flat rectangular wings of different aspect ratios are suddenly set into a constant forward speed at $\alpha = 5°$. The results of the present program are compared with the ones from [10]. The characteristics of the test are given in table [4.1].

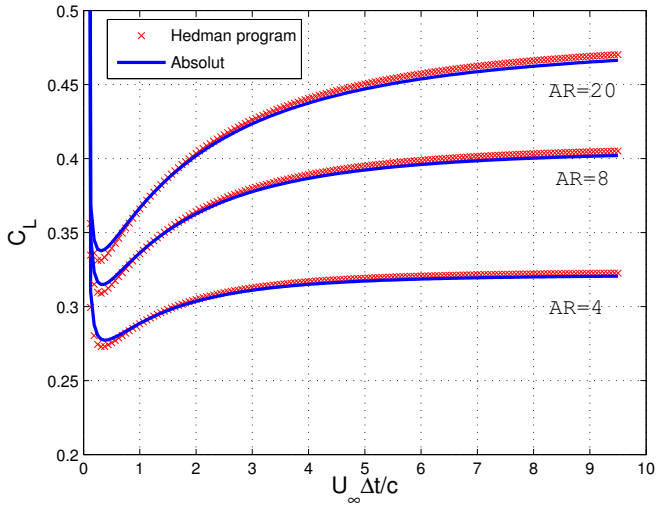

Figure 4.3: Lift coefficient for sudden acceleration of a flatplate

Variable	Value
n_x	4
n_y (b/2)	12
$U_\infty \Delta / c$	1/16
n_{steps}	152

Table 4.1: Sudden acceleration data

It is appreciated in Fig. 4.3 that the curve from Absolut, differs slightly from Hedring.

4.3 Heaving motion

The periodic lift has been calculated for a rectangular flat plate in heaving oscillation at a reduced frequency of $k = 0.5$ and an amplitude of $h = 0.1\ m$. The rest of characteristics of the flat plate and the motion are stated in table [4.2].

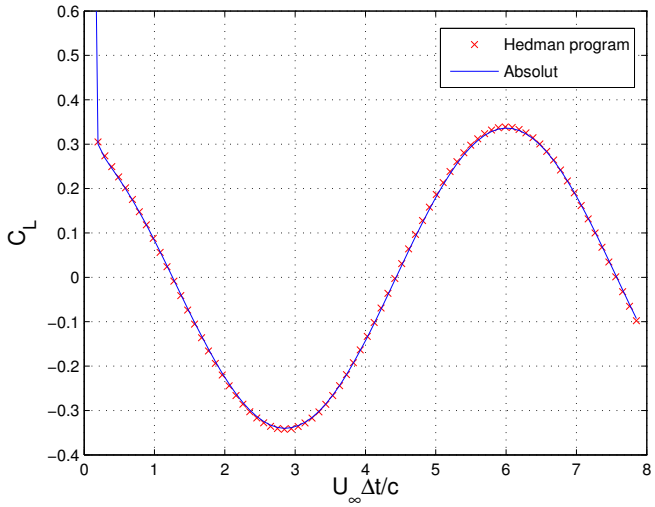

Figure 4.4: Lift coefficient for heaving motion of a flatplate at $k = 0.5$.

Fig. 4.4 depicts the evolution of the lift coefficient with time. An initial unrealistically large lift coefficient suffers a drop after the first time step because the wake shedding starts. In the next time steps, it becomes steady, following a harmonic undamped motion. The two set of computational methods give exactly the same results. The only exceptions are located at the top and the bottom of the curve, where the present method gives slightly lower lift coefficients.

Variable	Value
AR	4
n_x	4
n_y (b/2)	12
$U_\infty \Delta / c$	1/16
α	0°
n_{steps}	80

Table 4.2: Heaving motion data

4.4 Flapping flap

The hinge moment for a full-span flap of 40% chord on a rectangular wing is calculated in this case. The rigid flap is oscillating at a reduced frequency $k = 0.47$. The results are compared with the ones in [10] and [26].

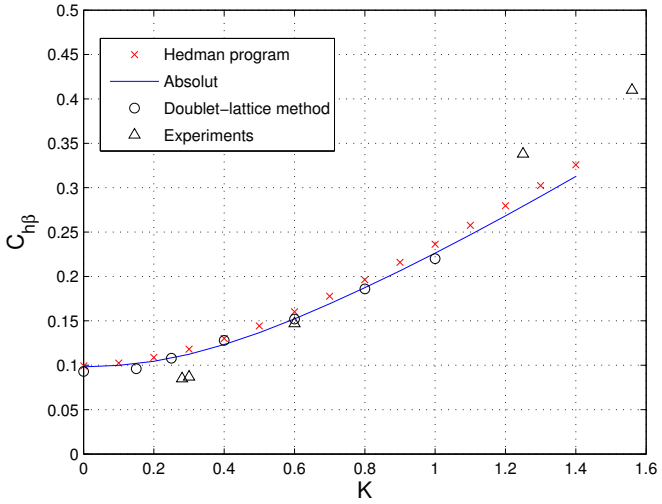

Figure 4.5: $C_{h\beta}$ for a wing with an oscillatory flap

In Fig. 4.5 the hinge moment coefficients of the different methods follow the trend of the experiments but they do not match them. It is interesting to point out that ABSOLUT solver fits the Doublet-lattice method while having a little gap with Hedring's. However, the three curves are quite similar.

Variable	value
AR	4
n_x	4
n_y (b/2)	12
α	0°
n_{steps}	80

Table 4.3: Flapping flap data

4.5 Bending wing

In the last test a flat plate oscillates in its first bending mode at $Mach = 0.24$. This corresponds, at sea level and standard atmospheric conditions, to $V_\infty = 82.7m/s$. The nondimensional amplitude is defined by Eq. (4.1).

$$h = 0.18043\,|(y/s)| + 1.70255(y/s)^2 - 1.13688\,\left|(y/s)^3\right| + 0.25387(y/s)^4 \tag{4.1}$$

where y/s is the relative span position. The rest of the data can be found in table 4.4. Fig. 4.6 shows pressure distributions in two sections of the wing. For the present method and Hedring, the pressures are calculated at $y/s = 0.0625$ and $y/s = 0.9375$. The experimental data are obtained in sections $y/s = 0$ and $y/s = 0.9$ from [26].

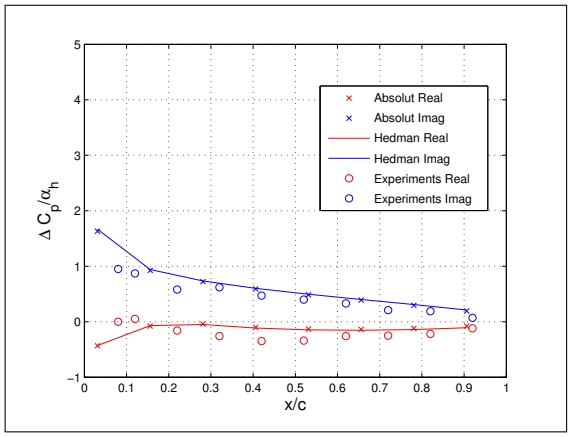

(a) Section $y/s = 0$

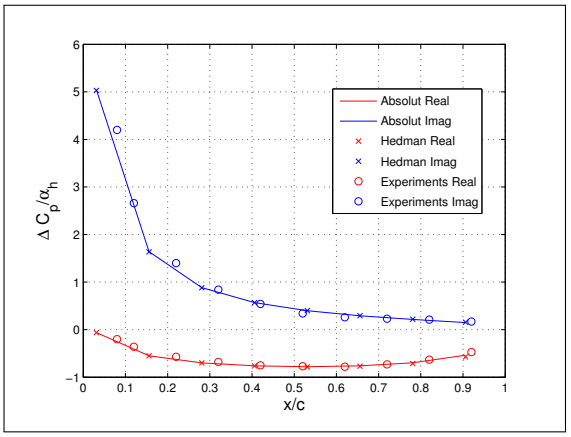

(b) Section $y/s = 0.9$

Figure 4.6: Pressure distributions for an oscillating wing

It is noticed in Fig. 4.6 that the numerical methods agree perfectly. With respect to the experimental case the agreement is also good. It is only noticeable the small gap between the results in Fig. 4.6a due to the difference between the sections in which the pressures have been calculated.

Variable	value
AR	3
n_x	8
n_y (b/2)	8
k	0.47
Mach	0.24
n_{steps}	80

Table 4.4: Bending wing data

4.6 Discussion of results

In all the previous cases ABSOLUT shows good agreement with the experimental data and almost perfect matching with Hedring. The last is expected since the present program is based on Hedring, so the calculations have been executed under the same conditions. Therefore, the code is proved to work for unsteady cases with simple geometries.

Chapter 5

Wind tunnel tests

'When the weight of the paper equals the weight of the airplane, only then you can go flying."

Attributed to Donald Douglas (Mr. DC-n)

In this chapter, the code is tested with experimental data obtained from wind tunnel measurements for two different configurations, a conventional aircraft and one with canard stabilizator. Tornado is included in this study in order to assure the goodness of ABSOLUT's calculations. To execute the analysis, a three-step approach has been designed; first, the geometric characteristics of the wind tunnel model are compared with the ones of the VLM model. Afterwards, ABSOLUT's results in steady conditions are contrasted with the ones from Tornado and the wind tunnel. The dependency on changes in the angle of attack and the sideslip angle are treated.

The last test aims to calculate unsteady derivatives with a reasonable accuracy. For the conventional configuration, the code is compared with the wind tunnel tests and computations of other programs. For the canard configuration, ABSOLUT is only proved against the experiments, as no other unsteady numerical calculations has been accomplished with other programs.

5.1 F12 configuration

DLR-F12 is a 1:29 scale aero-model based on an Airbus A-320. It was chosen for CEASIOM wind tunnel tests as an airplane with conventional configuration. All the information about the test campaign can be found in [13]. It does not have any control surface as it can be appreciated in Fig. 5.1. The main geometric characteristics of the model are presented in table 5.1 in comparison with the VLM models in Tornado and in ABSOLUT:

	Wind tunnel	Tornado	ABSOLUT
$S_{ref}(m^2)$	0.444	0.450	0.450
$\bar{c}(m)$	0.253	0.257	0.257
$b_{ref}(m)$	2.018	2.040	2.040
Ref. point x (m)	1.040	-	-
Ref. point y (m)	0	-	-
Ref. point z (m)	-0.030	-	-

Table 5.1: Comparison of fundamental geometrical data of F12

Table 5.1 presents no difference between Tornado and ABSOLUT geometry definition. Nevertheless, when considering the aero model, there are slight deviations for the VLM aircrafts but they are not large enough to suppose a difference for the calculations. About the reference point, it is important to point out that, since it is an input variable, it has only to be adjusted according to the given data. However,

some geometrical data are missing. The main one is the type of airfoils used, so NACA0012 are selected. Then, the model for the computations is regarded as an approximation not as good as it would be desired.

Figure 5.1: F12 model in wind tunnel

5.1.1 Steady results

To evaluate the steady characteristics of the DLR-F12 the sweep in the angle of attack α has been considered first. In Fig. 5.2, both Tornado and ABSOLUT curves are superimposed. However, there is a gap between experimental and numerical results as well as a difference in the slope. This can be explained from the airfoils used. As NACA0012 do not have camber is reasonable to expect that the lift is lower than in the wind tunnel model. Deviations shown in Fig. 5.3 are not so significant because the parasite component of the drag increase the total drag in the experimental data.

The lateral force, roll moment and yaw moment have no changes for different angles of attack. Hence, they are not plotted in any graph. The analysis of the pitch moment coefficient in Fig. 5.4 shows that Tornado and ABSOLUT follow the trend of the experimental pitch coefficient though there is a considerable difference in the slope. The computation curves cut the experimental data at $\alpha = 3°$.

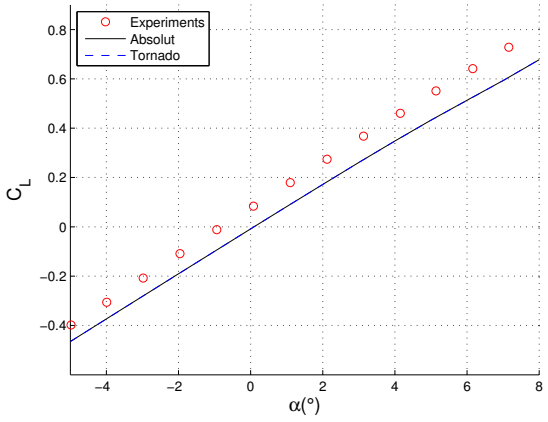

Figure 5.2: Lift coefficient variation for a sweep in α

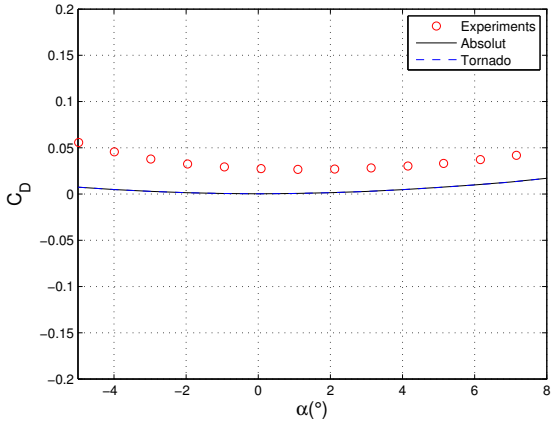

Figure 5.3: Drag coefficient variation for a sweep in α

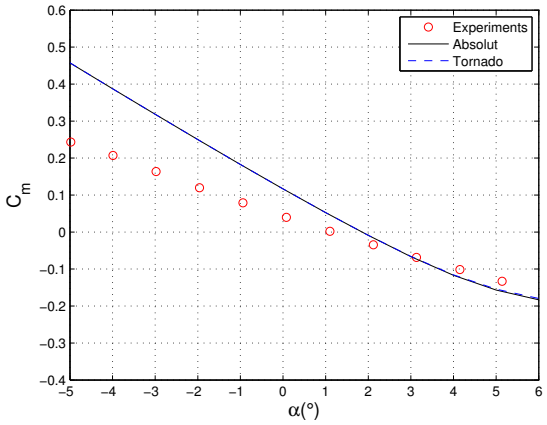

Figure 5.4: Pitch moment coefficient variation for a sweep in α

Figs. 5.5, 5.6 and 5.7 show the effects of a sweep in the sideslip angle β for an angle of attack $\alpha = 3.11°$. There is a considerable difference in the slope of the lateral force between the computational methods and the wind tunnel results., Fig. 5.5. Since Tornado and ABSOLUT do not consider the fuselage in the calculations, the deviation is expected. Also, the fuselage effect is even more noticeable for the calculation of the lateral moments of Figs. 5.6 and 5.7. Since there is no variation of the longitudinal forces and moments for a sweep in the sideslip angle, figures of them have been neglected.

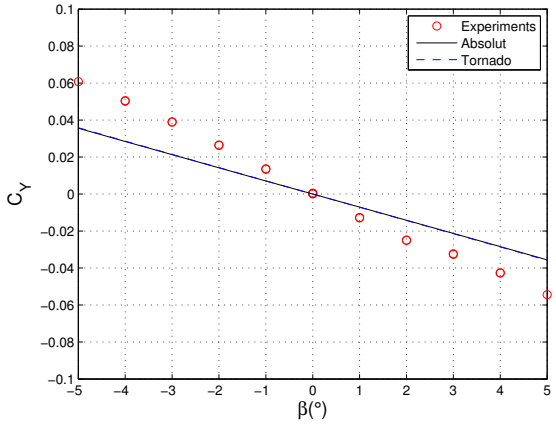

Figure 5.5: Lateral force coefficient variation for a sweep of the sideslip angle β

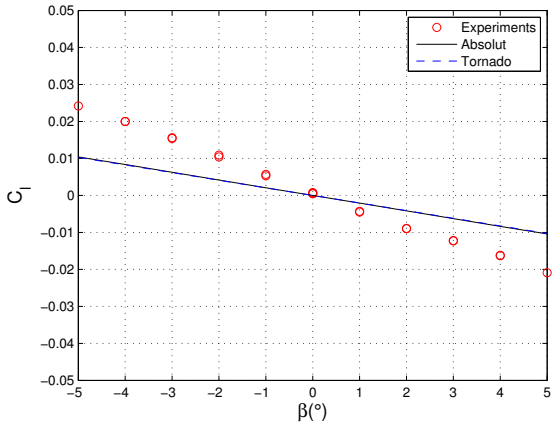

Figure 5.6: Roll moment coefficient variation for a sweep of the sideslip angle β

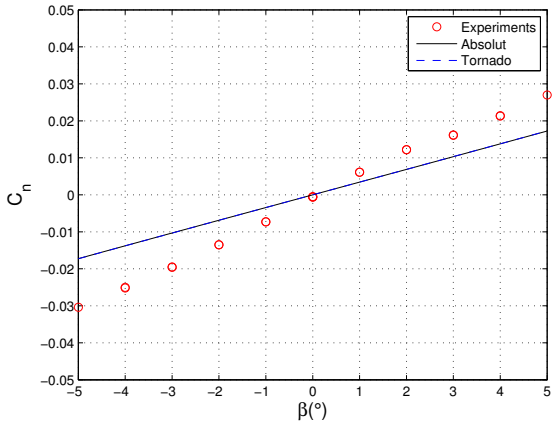

Figure 5.7: Yaw moment coefficient variation for a sweep of the sideslip angle β

5.1.2 Unsteady results

The last step of ABSOLUT test with respect to F12 is the unsteady analysis, which is its ultimate goal. Table 5.2 shows results for a pitching motion of the aircraft for a frequency $f = 3Hz$, an equilibrium angle $\alpha = 0°$ and an amplitude $\Delta\alpha = 4.52°$. Calculations performed by other codes are also present in the table. The first two columns refer to the steady stability derivatives, which have considerable deviations between experimental an numerical methods. The force and moment derivatives due to a change in the pitch rate show agreement in the numerical results. They have calculated under the quasi-steady assumption. In which respect to ABSOLUT's results for the unsteady derivatives, it matches the experimental results with a reasonable accuracy.

	$C_{L\alpha}$	$C_{m\alpha}$	C_{Lq}	C_{mq}	$C_{Lq} + C_{L\dot{\alpha}}$	$C_{mq} + C_{m\dot{\alpha}}$
DLR exp. data	5.77	-2.25	0.00	0.00	9.30	-24.24
DLR Euler	5.62	-2.29	7.15	-19.76	6.45	-25.10
DLR NS	4.97	-1.59	6.65	-17.90	6.30	-22.71
ONERA NS	5.40	-1.83	6.28	-17.86	5.88	-22.44
TsAGI	5.30	-1.99	6.99	-18.40	7.19	-24.01
ABSOLUT	5.20	-3.72	7.68	-19.92	8.10	-23.23

Table 5.2: Results for pitch motion test on F12 model for $\alpha_0 = 0°$, $\Delta\alpha = 4.52°$ and $f = 3\ Hz$

The results for a roll motion with frequency $f = 3Hz$ at angle of attack $\alpha = 6°$ and an amplitude $\Delta\phi = 4.52°$ are compared in table 5.3. As they are calculated under the quasi-steady assumption, there are no disturbances due to the wake. While the roll C_{lp} and yaw moments due to the rolling motion match the experimental moments accurately.

	C_{Yp}	C_{lp}	C_{np}
DLR exp. data	0.46	-13.97	-3.34
DLR Euler	0.97	-14.41	-4.46
DLR NS	0.86	-13.96	-4.05
ONERA NS	-0.67	-14.61	-3.34
TsAGI	-0.56	-14.81	0.76
ABSOLUT	0.34	-14.61	-3.06

Table 5.3: Results for roll motion test on F12 model for $\alpha_0 = 6°$, $\Delta\phi = 4.86°$ and $f = 3\ Hz$

The last test performed for the DLR-F12 is a harmonic yaw motion at angle of attack $\alpha_0 = 6°$, $\Delta\beta = 4.32°$ and $f = 3\ Hz$. The equilibrium sideslip angle is $\beta = 0$. Some differences are appreciated in the three first columns where the values dependent on the yaw angle are shown. For the unsteady derivatives, the deviations keep high. Since the VLM has no fuselage, these results are expected.

	C_{Yr}	C_{lr}	C_{nr}	$C_{Yr} + C_{Y\dot{\beta}}$	$C_{lr} + C_{l\dot{\beta}}$	$C_{nr} + C_{n\dot{\beta}}$
DLR exp. data	-	-	-	3.59	4.50	-9.65
DLR Euler	2.45	6.71	-9.47	-	-	-
DLR NS	2.28	6.25	-8.86	-	-	-
ONERA NS	-2.37	-4.81	6.28	-	-	-
TSAGI	3.32	2.69	12.38	-	-	-
ABSOLUT	1.75	3.89	-6.8	1.48	3.20	-5.76

Table 5.4: Results for yaw motion test on F12 model for $\alpha_0 = 6°$, $\Delta\beta = 4.32°$ and $f = 3\ Hz$

5.2 TCR-C15 configuration

The **T**rans **C**ruiser **A**ircraft (TCR) is a virtually designed aircraft. It is meant to be a civil transport airplane at substantial transonic speed. Within its mains features there is an integrated form with low wetted area, fuel-efficient transonic cruise and low noise radiation. The main characteristic of the C15 configuration is the canard in the front part of the fuselage. The model is a 1:40 scale down version of the aircraft. As with the F12, its main geometrical features are compared with Tornado and ABSOLUT definition.

Figure 5.8: TCR general configuration

In table 5.5 the geometry for the TCR-C15 wind tunnel model is compared with the geometry of the VLM model. All the parameters coincide with the exception of the mean aerodynamic chord $\bar{c}$. Since this fact only means that in the wind tunnel model that chord is calculated with a different definition from Tornado and ABSOLUT, next results for both Tornado and ABSOLUT are normalized for that chord. The point used as a reference for the moments, as for the DLR-F12, is defined according to the TCR-C15 model data.

	Wind tunnel	Tornado	ABSOLUT
$S_{ref}(m^2)$	0.306	0.306	0.306
$\bar{c}(m)$	0.294	0.404	0.405
$b_{ref}(m)$	1.12	1.116	1.116
Ref point for the moments (m)	0.874	0.874	0.874

Table 5.5: Comparison of fundamental geometrical data of TCR-C15

It is important to point out that, for this aircraft, there are no missing data. All the geometry is well known, including the different airfoils used in the wings. All the experimental data are obtained from [7].

5.2.1 Steady results

Here, the steady coefficients form the numerical methods match the experimental results almost perfectly in Fig. 5.9. For the pitch moment coefficient, however, the curves from ABSOLUT and Tornado only follow its trend. It is noticeable that ABSOLUT fits much better the experimental set of data in Fig. 5.10 than Tornado. This may be due to the addition of the real mean camber line to the vortex rings unlike in Tornado, where only the normals of the airfoil are defined.

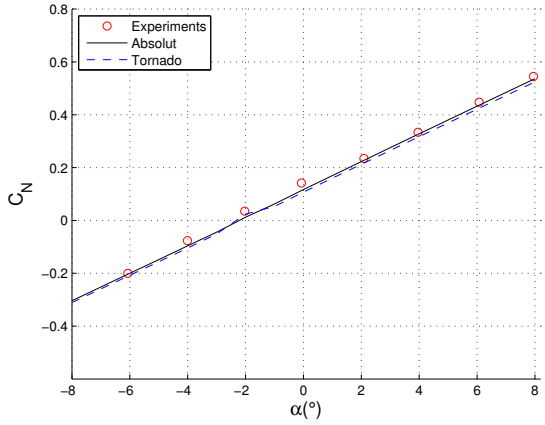

Figure 5.9: Normal force coefficient vs angle of attack at $V_\infty = 40\ m/s$

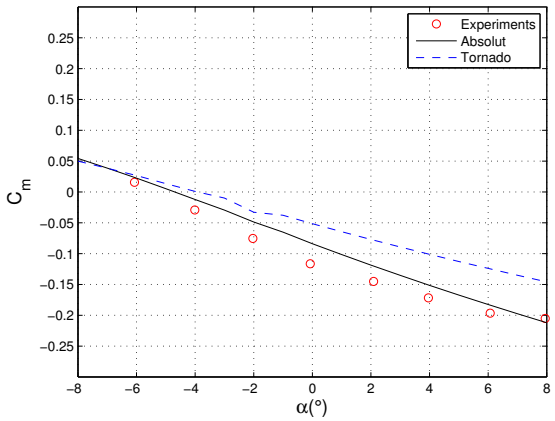

Figure 5.10: Pitch coefficient vs angle of attack at $V_\infty = 40\ m/s$

To analyze the sweep in the sideslip angle $\beta = -8 : 8°$ at an angle of attack $\alpha = 6°$ (no lower value is available) the variations of the lateral forces and moments are described in the next three figures. In Fig. 5.11 the lateral force show different slopes between the numerical and the experimental curves. However. the moments in Figs. 5.12 and 5.13, both ABSOLUT and Tornado are much closer to the wind tunnel data. It is noticeable that the roll moment and the lateral force coefficients are calculated more accurately with Tornado.

Unlike the DLR-F12 model, in the TCR-C15 the computations have close agreement with the experimental results. This is caused by the accurate VLM geometry used in this case.

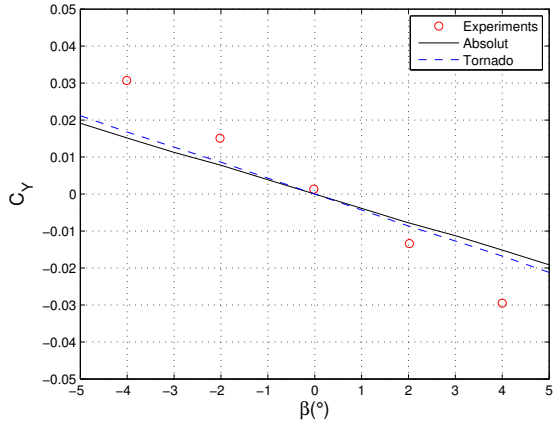

Figure 5.11: Lateral force coefficient variation for a sweep of the sideslip angle β

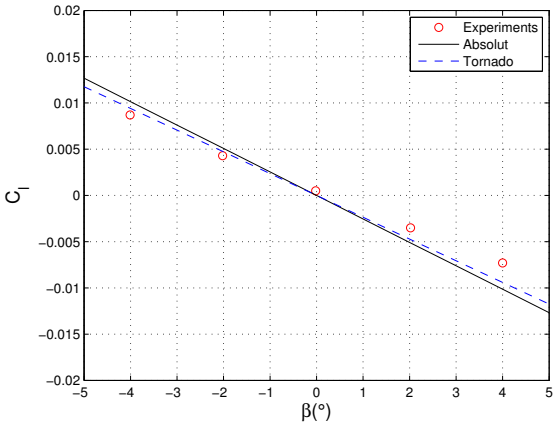

Figure 5.12: Roll moment coefficient variation for a sweep of the sideslip angle β

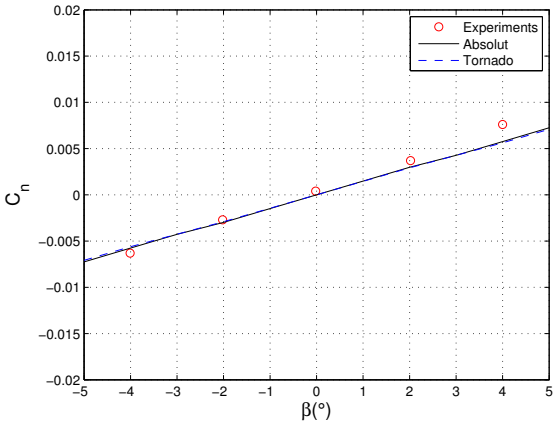

Figure 5.13: Yaw moment coefficient variation for a sweep of the sideslip angle β

5.2.2 Unsteady results

For the unsteady analysis of the TCR-C15 configuration, longitudinal moments and forces have been tested. ABSOLUT also obtains good approximations for the dynamic derivatives in TCR.

	$C_{L\alpha}$	$C_{m\alpha}$	C_{Lq}	C_{mq}	$C_{Lq}+C_{L\dot{\alpha}}$	$C_{mq}+C_{m\dot{\alpha}}$
SIMSAC exp. data	2.86	-0.97	-	-	7.02	-5.78
Tornado	3.03	-0.75	4.19	-6.30	-	-
ABSOLUT	3.03	-1.03	4.28	-6.28	7.72	-5.56

Table 5.6: Results for pitch motion test on TCR-C15 model for $\alpha_0 = 0°$, $\Delta\alpha = 3°$ and $f = 1\ Hz$.

For this case, a core size of $k_{wing} = 1$ has been used to smooth the wake and a core size of $k_{wake} = 0.5$ has reduced the disturbances in the wing. The explanation for this circumstance is that, in the canard configuration, the instabilities produced in the solution by the wake are much larger than in the conventional aircraft. The lifting surfaces are much closer in TCR VLM model than in F12's, as it can be appreciated in Fig. 5.15. Also, the tip vortices of the canard have to be accounted. Therefore, the interaction wake-wing is higher in the TCR motion so a higher core size ϵ has to be used in Biot-Savart equation, see section 3.3.6. To obtain proper factors k, an empirical approximation has been followed. It starts with $k_{wing} = 1$, which has been found to be a good value to smooth the influence of the wing on the wake. For the value k_{wake}, it has been increased successively until the instabilities in the forces disappear. In TCR-C15, for a pitch harmonic motion, the normal force was observed, as its high resultant with respect to the other forces make it easier to analyze. In Fig. 5.14, it can be appreciated that, for the same oscillatory pitch motion, the instabilities in the solution have been smoothed by establishing different core sizes for the wake and wing vortex rings.

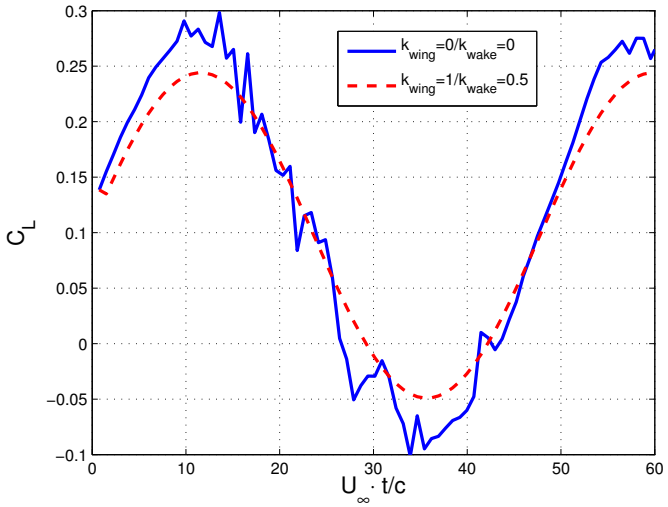

Figure 5.14: Lift coefficient variation with time for TCR-C15 in oscillatory pitch motion at $\alpha_0 = 0°$, $\Delta\alpha = 3°$ and $f = 1\ Hz$.

5.3 Agreement between ABSOLUT and the experimental results

With respect the DLR-F12 case, the steady results have considerable differences with respect to the experimental ones. The two main reasons are lack of camber in the airfoils, which applies to all the forces, and lack of fuselage effects, which mainly affects lateral forces and moments. In spite of this situation, the unsteady stability derivatives have matched reasonably the data from the wind tunnel tests, selecting a core size $k = 0.1$ to stabilize the wake.

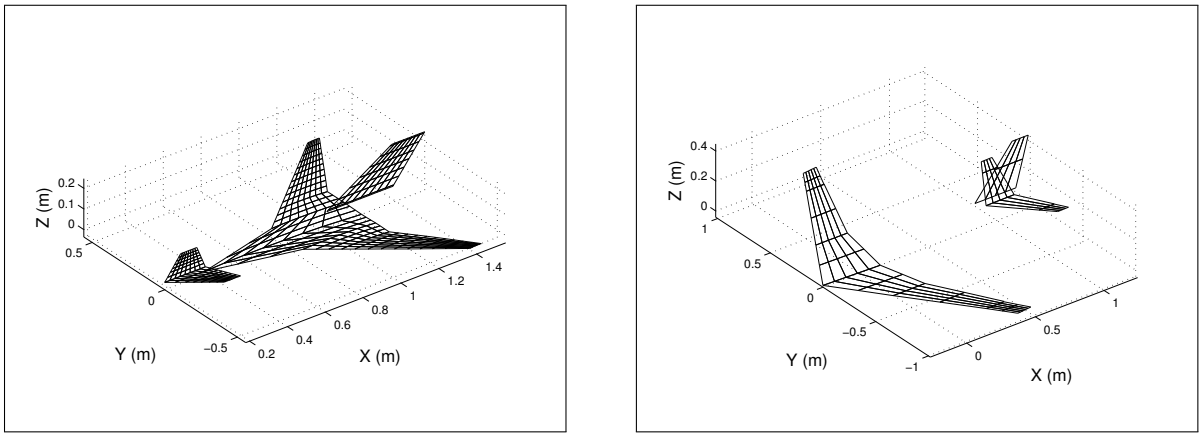

(a) TCR-C15 model

(b) DLR-F12 model

Figure 5.15: Comparison between the TCR configuration and the DLR-F12

For the TCR-C15 configuration the situation is different. The geometry is known so the computations match almost perfectly the experiments under steady and quasi-steady conditions. For the dynamic derivatives there is also good agreement.

Chapter 6

Conclusions

"And yet it moves"

Attributed To Galileo Galilei, scientist

From the results shown in chapter 4, it can be concluded that ABSOLUT is able to calculate aerodynamic coefficients for simple geometries under unsteady conditions. An special case has been the elastic motion of a wing in its first bending mode. Since the results match the experiments, it can be assured that elastic motion of a wing can be achieved as an extension for the present program. Also, the oscillating flap case shows another kind of motion relative to the wing coordinate system. The success in this case can be regarded as another proof of the goodness of ABSOLUT for solving relative motions in unsteady conditions. As only slight deviations from experimental and other computational methods have been obtained, the first statement is considered proven.

ABSOLUT has also been checked for steady computations of modern aircraft configurations. In this calculations, the present method has shown that is as accurate as Tornado, the steady vortex lattice method in which ABSOLUT is based on. Nevertheless, some remarkable results have arisen; when the aircraft has non-symmetric airfoils, the results from the present code differ from the ones of Tornado. Specifically, the longitudinal forces and moments solutions calculated by ABSOLUT become closer to the wind tunnel data. Then, the modification of the wing geometry according to the mean camber line can be stated as useful. In spite of these facts, the code can be regarded as equivalent to Tornado.

In the unsteady cases, the program accuracy depends on the aircraft configuration. For the classical configuration (DLR-F12) provides reasonable approximations to the experiments for longitudinal dynamic derivatives. When obtaining the lateral derivatives, the fuselage influence is cause of higher disagreements with the real model results. It is noticeable that, for the DLR-F12, the lack of geometrical information affects, mainly, the steady derivatives calculation. When TCR-C15 is studied, the results are much more accurate. The reason for this agreement is a better knowledge of the geometry. However, the wake-wing interactions are higher for this type of aircraft, due to a close distance between the canard and the main wing as well as the effect of the tip vortices of the canard. Therefore, it is affirmed that canards configurations need higher corrections in the wake as well as in the wing calculations by using a higher core size than in conventional configurations (as DLR-F12).

The well tested steady wake model provides the expected results. The unsteady wake proportionates also accurate results, although its modeling has some drawbacks. The main ones are the stretching and torsion of the vortex rings, which do no fulfill the angular momentum equation.

In the end, it can be stated that ABSOLUT is an unsteady Vortex Lattice method that calculates with reasonable accuracy the dynamic derivatives.

Chapter 7

Acknowledgments

I would like to thank Arthur Rizzi for giving me the chance of doing this master thesis at the Aerodynamics division of KTH. His guidance during all these months has encouraged me to proceed on my thesis. Also, I acknowledge Jesper Oppelstrup for his technical and theoretical advices, which have been invaluable. To both of them, I specially thank for approaching my doubts and difficulties with patience and kindness.

I would like also to thank Sven Hedman. His code has proved to be really helpful for my thesis.

I am also grateful to the people with whom I have worked because of the environment that they have created in the office. I cannot forget either Carlos, Victor, Mario and Julio, whom were there for me in my failures and in my successes. But I am specially thankful to my girlfriend, my main source of support and joy.

At last but not the least, I thank my family for all their support during, not only these months, but my whole life.

-

Most of the bibliographic entries of SimSAC can be downloaded from
‘‘http://www.simsacdesign.org/’’.

Bibliography

[1] Anderson, J.D., *"Fundamentals of Aerodynamics,"* McGraw-Hill Editions, 3^{rd} edition, 2001.

[2] Bertin, J.J., Smith, M.L., *"Aerodynamics for engineers,"* Prentice-Hall, 1989.

[3] Borglund, D., Eller, D., *"Aeroelasticity of Slender Wing Structures in Low-Speed Airflow,"* KTH, Aeronautical and Vehicle Engineering Department, 2010.

[4] Drela, M., *"ASWING 5.81 Technical Description - Unsteady Extension,"* MIT, 2008.

[5] Etkin, B., Loyd, D.R., *"Dynamics of Flight,"* John Wiley & Sons, Inc., 1996.

[6] Feynman, R.P., Leighton, R.B., Sands, M., *"The Feynman lectures on Physics,"* Addison-Wesley, Vol. 2, 1964.

[7] Khrabrov A., Kolinko K., Zhuk A., Grishin I., *"Simulating Aircraft Stability and Control Characteristics for Use in Conceptual Design,"* SimSAC report,TsAGI, 2006.

[8] Goetzendorf-Grabowski, T., *"Coordinates, signs and units definition,"* SimSAC, 2009.

[9] Gülçat, Ü. *"Fundamentals of Modern Unsteady Aerodynamics,"* Springer, 2010.

[10] Hedman, S., *"Calculations of Unsteady Aerodynamics for Wings in Incompressible Flow,"* Hed PM 960301.

[11] Hedman, S., *"Unsteady Flows around Oscillating Wings in Incompressible Flow,"* KTH.

[12] Hübner, A., *"WP4: Benchmark Aerodynamic Model,"* SimSAC, Technical Meeting, ONERA, Lille, 2008.

[13] Hübner A.R. *"Steady / Unsteady Force and Pressure Measurements of the DLR-F12 model in the DNW-NWB within the European Research Project SimSAC,"* SimSAC report, Braunschweig, Institute of Aerodynamics and Flow Technology, 2008.

[14] Karamcheti, K., *"Principles of Ideal-Fluid Aerodynamics,"* Krieger Pub Co, 2nd edition, 1980.

[15] Karlsson, A., *"Lectures notes in SD2601:Fundamentals of Flight,"* KTH, Aeronautical and Vehicle Engineering Department, 2009.

[16] Katz,J., Plotkin, A., *"Low Speed Aerodynamics: From Wing Theory to Panels methods,"* McGraw-Hill Editions, 1991.

[17] Kolbe, C. D. and Boltz, F. W., *"The Effect at High Subsonic Speeds of a Flap-Type Aileron on the Chordwise Pressure Distribution Near Mid-Semi-Span of a Tapered 35Â° Swept-back Wing of Aspect Ratio 4 Having NACA 65A006 Section,"* RM A51G31, NACA, 1951.

[18] Maričić, N., *"Software development for subsonic aircraft's unsteady longitudinal stability derivatives calculation,"* Theoret. Appl. Mech., Vol.32, No.4, pp. 319-340, Belgrade 2005

[19] Maričić, N., *"Numerical estimation of aircrafts' unsteady lateral-directional stability derivatives,"* Theoret. Appl. Mech., Vol.33, No.4, pp. 311-337, Belgrade 2006

[20] Mialon, B., Ben Khelil, S., *"Numerical simulations of the derivatives, CFD work,"* ONERA, 2008.

[21] Melin, T., *"A Vortex Lattice MATLAB Implementation for Linear Aerodynamic Wing Applications,"* KTH, 2000.

[22] Meseguer Ruiz, J., San AndrÃ©s, A., *"AerodinÃ¡mica bÃ¡sica,"* Springer, 2010.

[23] Molitor, P., *"Extending the Tornado Vortex Lattice Method for Stability Analysis using the CEASIOM software,"* KTH, 2009.

[24] Moran, J., *"An Introduction to Theoretical and Computational Aerodynamics,"* Dover Publications, 1991.

[25] Rizzi, A., *"Background Documentation for Software&Labwork Course SD2610: Computational Aerodynamics in Aircraft Design,"* KTH, Aeronautical and Vehicle Engineering Department, 2009.

[26] Rodden, W.P., Albano, E., *"A Doublet-Lattice Method for Calculating the Lift Distribution on Oscillating Surfaces in Subsonic Flow,"* AIAA Journal, Vol. 2, No. 7, 1969.

[27] Wright, J.R., Cooper, J.E., *"Introduction to Aircraft Aeroelasticity and Loads,"* John Wiley & Sons, Ltd., 2007.

[28] *"SimSAC: Task 4. Comparison of experimental and numerical results, "* SimSAC.

[29] *"NACA Airfoil Series,"* Aerospace Web, http://www.aerospaceweb.org/question/airfoils/q0041.shtml (, accessed August, 2011.)

[30] *"CEASIOM,"* CEASIOM project website, http://www.ceasiom.com/ (, accessed September, 2011.)

[31] Simsac project website. http://www.simsacdesign.org/ (, accessed September, 2011.)

[32] *"Redhammer"* http://www.redhammer.se/ (, accessed August, 2011.)

[33] *"XFOIL,"* http://web.mit.edu/drela/Public/web/xfoil/ (, accessed April, 2011.)

[34] *"Nearinc, Shaman developers,"* http://www.nearinc.com (, accessed July , 2011.)

[35] Mason, W.H. *"Applied computational aerodynamic text/notes"* http://www.dept.aoe.vt.edu/~mason/Mason_f/CAtxtTop.html (, accessed May , 2011.)

Appendix A

Code structure

In this appendix there is a brief explanation of the different functions of the code as well as how they are related to each other.

- **main.m**: Script of unsteady potential solver. This file calls the different functions for steady and unsteady problems. Calls: fgeo, fstate, presolver and postpro.
- **fgeo.m**: It is the geometry input function of the program. Called from main.m. Calls: nothing. Inputs: it does not have.
- **fstate.m**: This function defines the flight conditions. Then, it gathers them in state array. Called from main.m.
- **presolver.m**: This function calls flattice and fsolver function accordding to the type of analysis chosen.. Called from main.m.
- **flattice.m**: It dicretizes the geometry, places the vortex rings and collocation points, calculates the panel normals, areas and also the reference parameters of the wing. Called from presolver.m. It calls prelattice.m, fcorner.m, tmesh.m, fring.m, supereval.m and fnormal.m.
- **prelattice.m**: It calculates the number of panels in each subdivision of the wing as well as the mean camber lines of the inboard and outboard airfoils and the sweep angle of the leading each of each partition. Called from flattice.m. It calls farfoil.m.
- **farfoil.m**: It calculates the mean camber line of the inboard and outboard airfoil of each partition. Called from prelattice.m.
- **fcorner.m**: It defines the partition by calculating its corner's coordinates in the wing system. Called from flattice.m.
- **tmesh.m**: Formerly TORNADO's function. It defines the partition mesh, given its corner points and number of panels in x- and y-directions, and the mesh type. Called from flattice.m.
- **fring.m**: This function defines the vortex rings and the panels on a discretized partition, considering the mean camber line of the different airfoils. Called from flattice.m.
- **fnormal.m**: Calculation of the panels normal and areas . Called from flattice.m.
- **fsolver.m**: This is the connector file for the iterative process that is performed to solve the unsteady problem. Called from presolver.m. Calls: ISAtmosphere, rotation, transformation, shedding, fcoeff, fgamma, fwake (when unsteady) and forces.
- **ISAtmosphere.m**: Formerly TORNADO's function. It provides, given a certain altitude, air density, speed of sound, static pressure and viscosity, all according to the International Standard Atmosphere tables. Called from fsolver.
- **rotation.m**: Calculation of the distance of the center of gravity and other reference points with respect to collocation points and vortex corners . Called from fsolver and from transformation.

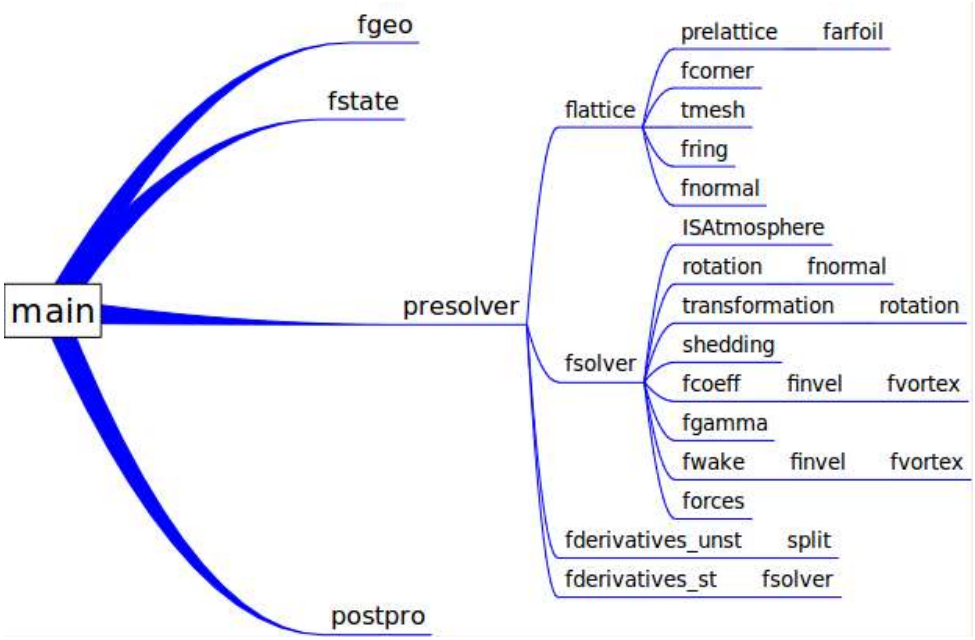

Figure A.1: Code structure

- **transformation.m**: Transformations between wing and inertial reference systems according to the defined motion of the wing. Called from fsolver. Calls rotation.
- **shedding.m**: Wake-shedding. Release of the wake vortices from the trailing edge of the wing in the inertial reference system according to the motion of the wing. Called from fsolver.
- **fcoeff.m**: This function calculates the influence coefficients matrix from the induced velocities in each collocation point. Called from fsolver. Calls: finvel.
- **finvel.m**: Arrangement of matrices to calculate the induced velocities.. Called from fcoeff. Calls fvortex.
- **fvortex.m**: This function calculates the velocity that a vortex segment induces in a certain point X,Y,Z by using the Biot-Savart law. Called from finvel.
- **fgamma.m**: This function calculates the vortex strength in each panel.Application of the solid-boundary condition. Called from fsolver.
- **fwake.m**: This function calculates the wake roll-up.
- **forces.m**: This function calculates the different aerodynamic parameters. Called from fsolver.
- **postpro.m**: This function provides plots and data from the results.Called from main.
- **fderivativesst.m**: This function calculates the steady derivatives through a central difference in the state of motion selected. Called from presolver. Calls fsolver.
- **fderivativesunst.m**: This function calculates the steady derivatives through a central difference in the state of motion selected. Called from presolver.
- **split.m**: Solves Harmonic motion in imaginary and harmonic part. Function reaimaJO, from Hedring, slightly modified. Called from fderivativesunst.

Appendix B

Some remarks on the DLR-F12 tests

It is not possible to reproduce directly some of the results given in chapter 5 for the DLR-F12 experiments. The reasons are related to the way the nondimenional system is defined in [13].

First at all, the reference length that is used for all the derivatives is the mean aerodynamic chord $\bar{c}$ of the airplane. This is the general choice for the longitudinal derivatives. However, in the calculation of the lateral ones it is usual to choose the span of the main wing b. ABSOLUT uses NASA system, as in [5].

The second source of change is the definition of the reduced frequency. In [13] is defined as in Eq. B.1. Then, the nondimensional dynamic derivatives in the cited test campaign are calculated in the same way as Eq. B.2. So, when calculating, the dynamic derivatives, they should be divided by two to match the experimental results.

$$k = \frac{\omega \bar{c}}{V_\infty} \tag{B.1}$$

$$C_{Lq} + C_{L\dot{\alpha}} = \frac{\partial C_L}{\partial \frac{q\bar{c}}{V_\infty}} + \frac{\partial C_L}{\partial \frac{\dot{\alpha}\bar{c}}{V_\infty}} \tag{B.2}$$

Appendix C

Future work

Next sections describe future tasks hat can be done to improve ABSOLUT:

C.1 C functions

Change fsolver.m and all its subfunctions to C programming language. This should decrease the computation time to the minimum as well as allow to change easily, in Matlab, the pre- and post- processors.

C.2 Gust field

Gust field influence on the aircraft. There is an interesting model in [4].

C.3 Aircraft propeller

It seems proper to add an unsteady model of a propeller as in reference [16]. The main features of this extension are:

- **Propeller definition**: Each rotor is defined as a new wing, with a certain number of blades. After one blade is generated, by symmetry, the new blades are created too.
- **Time step**: Since the propeller rotation velocity is much higher than the airplane's one, its time-step has to be smaller, which means that for each iteration in the solver, the rotor sheds more rows of vortex rings than the aircrafts (only one).
- **Vortex tubes**: It seems that an adequate model for the propeller's lattice, for the Biot-Savart's Law, involves vortex tubes instead of vortex lines.

C.4 Flexible wing

An initial stage of this development has been done in the chapter 4.

C.5 Aeroelasticity

Since the aerodynamic model is already developed, a structural model is left. However, further research has to be done in order to specify the characteristics of the structural models and their interaction with the aerodynamics.